JMEPEG
https://doi.org/10.1007/s11665-024-09533-0

1059-9495/$19.00

ORIGINAL RESEARCH ARTICLE

Performance Studies on the Wire Electric Discharge Machining Characteristics of Stellite-6B Superalloys

Rajashekhar Hosalli, S.P. Shanmuganatan, and M. Madhusudan

Submitted: 27 November 2023 / Revised: 24 February 2024 / Accepted: 30 March 2024

Wire electric discharge machining (WEDM) is a specialized, electrothermal, nontraditional process to machine complex shapes. The aim of this research is to optimize the WEDM operating attributes with the objective of achieving a maximum material removal rate (MRR) and minimum roughness of the machined surface (Ra) for a stellite (6B grade) alloy. Taguchi experimentation (L_{27}) was carried out to determine the influence of machining attributes on the output responses. The influence of process attributes was studied using an analysis of variance (ANOVA) concatenated with grey relational analysis and the fuzzy logic concept. Scanning electron microscopy was performed to characterize the recast layer on the machined surface. Based on multiple objective criteria for achieving the maximum MRR and minimum Ra, the optimal coalition of process attributes was 80 μs pulse-on time, 10 μs pulse-off time, 3 m/min wire feed rate, 5 A peak current and 40 μm/s bed speed.

Keywords material removal rate, scanning electron microscopy, stellite-6B superalloy, surface roughness, wire electric discharge machining

1. Introduction

Machining procedures eliminate undesirable material from a large work piece, introducing the final product's shape. Machining by traditional methods involves the generation of forces by cutting tools, causing the material to plastically deform. This plastic deformation results in the separation of chips (Ref 1). In light of the outstanding purposes and challenges faced in traditional machining of super alloys, the present investigation focuses on one such nontraditional approach to circumvent these issues and challenges. The versatility and viability of manufacturing through wire electric discharge machining (WEDM) pave the way for effective and efficient techniques for machining difficult-to-cut materials. WEDM is an important technique for cutting conductive materials to generate complicated profiles. Material removal occurs as a result of melting and evaporating of the workpiece caused by heat generated by discharge.

During WEDM, high-energy electrical discharges results in localized heat generation leading to the formation of heat-affected zone around machined surface. Excessive heat can cause changes in the material structure with the formation of microcracks and recast layer, thereby affecting the surface integrity. Specific conditions that promote better surface quality in WEDM include optimized pulse parameters, dielectric fluid selection, wire material and optimized cutting strategy. Small pulse durations and lower pulse energies can often result in finer surface finishes. Using deionized water with dielectric properties can help in achieving better surface quality. Finer wires typically result in smoother surface due to their ability to create finer features. In view of this, present investigation focuses on the optimization study to achieve ideal combination of machining parameters, which could embark on the surface integrity.

Stellite alloys are an amalgamation of cobalt-chromium super alloys that are suitable for high wear resistance and superior chemical and corrosion resistance in hostile environments. Stellite alloys are considered to be difficult to machine due to their hardness and toughness compared to those of other metals and alloys. Hence, the machining of these materials has become more expensive. Furthermore, stellite alloys consist of hard carbides, a nonhomogeneous crystal structure, a nonhomogeneous distribution of carbides, a high heat-affected zone and additional residual stress, resulting in poor machinability. Due to work hardening/strain hardening, notch wear can occur on the tool during machining. Burr forms on the strain-hardened layers, leading to fracture on the insert edge. During machining, high strength is sustained at elevated temperatures, opposing the plastic deformation needed for chip formation. The occurrence of tough and continuous chips degrades the cutting process by seizure and cratering effects. A high temperature is generated at the tool tip, resulting in tool wear. Stellite alloys undergo work hardening and retain the majority of their strength during machining, resulting in an increase in thermal stress. During machining, there is a localization of shear in the chip, which produces saw-tooth edges. These alloys tend to weld with tool materials at higher temperatures. Additionally, the hottest spot is the tool tip, which is at least some distance from the tool cutting tip, resulting in rapid tool wear. Hence, the wire EDM process overcomes machining limitations and is advantageous for processing these alloys.

Rajashekhar Hosalli, S.P. Shanmuganatan, and **M. Madhusudan**, Department of Mechanical Engineering, Dayananda Sagar College of Engineering, Bengaluru, Affiliated to Visvesvaraya Techological University, Belagavi 590018, India. Contact e-mail: kashyapa.madhu@gmail.com.

Published online: 08 May 2024

Owing to their desirable properties, such as superior strength, toughness, resistance to wear, fracture and corrosion characteristics, the demand/momentum of stellite alloys has increased because of their ability to be applied in industrial and commercial fields such as aerospace, nuclear waste storage, automobile sectors and surgical implantations. Stellite 'B' improves the performance of aircraft engine components such as flare castings, spacer sleeves, rod end bearings, ball bearings, bearing races, fuel nozzles, swirlers, washers, engine vanes, turbine blades, bearing supports and other static structural parts.

Kuldeep Singh et al. (Ref 2) studied the influence of pulse on, pulse off, wire type (soft brass- and zinc-coated diffused wire) and peak current on die steel H-13 material using WEDM. The machining was assessed for its cutting performance using ANOVA in terms of Ra and MRR. The study concluded that pulse-on and pulse-off factors exert a significant influence on MRR. With regard to Ra, pulse-on time is significant compared to other parameters.

Titus Thankachan (Ref 3) evaluated the machining characteristics of friction stir-processed copper BN composites during the WEDM process in terms of pulse-on, pulse-off and boron nitride volume fractions by adopting the L_{27} orthogonal array method. The MRR and surface roughness were measured as the output response. Optimization was performed using ANOVA. The evaluation concluded that the MRR is significantly influenced by the pulse-on and volume fractions and that the pulse-off has the greatest influence on the attainment of the minimum Ra values. Soorya Prakash et al. (Ref 4) investigated the sliding wear characteristics of multiwalled carbon nanotube (MWCNT)-reinforced copper metal matrix composites through experimentation and statistical and artificial neural network approaches. An L_{16} orthogonal array was implemented, and parametric optimization was accomplished via Taguchi analysis. The outcomes of the ANN closely correlated with the ANOVA findings.

Harvinder Singh et al. (Ref 5) investigated the effect of WEDM variables on surface roughness of AISI H13 using the ANOVA method. The optimal sets of process attributes to achieve better surface finish are arrived at. The investigation unveiled that wire type and pulse-on time are the most influential factors for surface roughness. The roughness parameter does not show changes with variation in wire tension.

Mandal et al. (Ref 6) employed Taguchi grey relational analysis to study multi-performance characteristics on WEDM of Al 7075 alloy using brass-coated wire electrode. ANOVA and percentage of contribution have been performed on grey relational grade to evaluate the influencing factors at 95% confidence level. Validation of predicted results is carried out by confirmatory experimentation. The analysis concluded that 52% of pulse duration and 27% of pulse interval are the most dominating factors having significance in respect of other factors.

Anand Shivade and Vasudev Shinde (Ref 7) proposed Taguchi grey relational analysis to study the optimization of WEDM process parameters for selected quality targets such as dimensional deviation, gap current and machining time. The study concluded that optimal combination formulated using analysis resulted in the grade increment of the order of 1.22%.

Rakesh Chaudhari et al. (Ref 8) employed a face-centered central composite design of response surface methodology (RSM) with grey relational grade to simultaneously optimize MRR and Ra of pure titanium. Experimental matrix was devised using RSM technique. The observation concluded that the optimized set of process parameters to maximize MRR and to minimize Ra were found to be pulse-on time of 6 μs, pulse-off time of 4 μs and discharge current of 6A during WEDM of solid pure titanium rod of diameter 10 mm.

Sathiskumar Jothi et al. (Ref 9) predicted the roughness and material removal rate factors via WEDM of aluminum-based composites by concatenating Taguchi, GRA and neural network modeling to determine the effectiveness of the developed models. The significant effects of pulse-on, pulse-off time and wire feed on the MRR and Ra were examined. The study concluded that the maximum MRR with the minimal Ra value can be obtained for an aluminum composite with 5 wt.%-SiC and 20 wt.%-Sn when operated under the conditions of 125 μs pulse-on, 40 μs pulse-off and a 7-m/min wire feed rate. Sabri Ozturk (Ref 10) studied the machinability of Grade 6 stellite using a turning operation. Machining was carried out using two different cutting tool materials (ceramics and tungsten carbide). The two materials were compared in terms of surface roughness at different speeds and feed rates. Experimental analysis revealed that whisker-reinforced ceramic inserts were more suitable than later inserts for the effective machining of stellite 6.

Yong Jia (Ref 11) studied the feasibility of near dry milling (EDM) of stellite alloys. The design of experts is used to assess the influence of the process on the performance assessment in terms of the material removal rate, tool wear rate and surface roughness. The study concluded that the discharge current has a significant effect on these parameters. Levent Urtekin et al. (Ref 12) applied WEDM to mill AZ91 alloys since the cutting tool applied no cutting pressure or plastic deformation to the product, resulting in an elevated temperature. In their study, WEDM caused the emergence of craters and small fissures on the outermost layers of samples due to liquid material melting, evaporation and fast solidification.

Using WEDM, Randeep Singh Gill and coworkers (Ref 13) reconstructed the surface characteristics and corrosion behavior of Mg-4Zn alloys. The parametric effects of machining with respect to the spark-on, spark-off time factor and servo voltage were discussed. The observation concluded that large surface craters, microcracks and micropores are the outcomes of increasing discharge energy during the machining process, leading to a greater order of surface roughness and corrosion. Nixon Kuruvila and Ravindra (Ref 14) studied the parametric influence and optimization of wire EDM characteristics of hot die steel. The input parameters of the study included pulse on, pulse off, bed speed and current. The output responses defined are the surface roughness and volumetric material removal rate. The study concluded that for higher pulse-on values, a higher MRR prevails, and constrained values are used to attain a good surface finish.

Tosun et al. (Ref 15) investigated the roughness parameters of a surface using machining parameters, namely pulse duration, voltage, wire feed and dielectric fluid pressure, on SAE steel. The investigation revealed that increasing the pulse duration, voltage and wire speed increased the surface roughness. Additionally, an increase in the fluid pressure of the dielectric medium improves the surface finish. Ramamurthy et al. (Ref 16) studied the effect of wire electrodes on the surface finish and kerfwidth using a Ti-Al-4 V alloy. An L_9 orthogonal array was constructed for the study with brass-, zinc- and brass-coated diffuse wire. The observation concluded that the surface finish with diffused coated wire is better than that with the latter.

Tripathy and Tripathy et al. (Ref 17) observed the influence of peak current, pulse-on time, powder concentration and duty cycle. The GRA and TOPSIS techniques were employed for optimizing the tool wear rate and material removal. The values optimized by GRA and TOPSIS are in good agreement. Using an experimental approach, Ramesh Raju et al. (Ref 18) investigated the optimum process parameters for attaining improved machining performance in Haste alloy C276 via EDM via the Taguchi design. The variables for the process include pulse on, pulse off and current. Material removal, surface finish and overcutting are significantly influenced by the current.

Balaji and Narendranath (Ref 19) machined Ni-rich Ni-Ti-Hf alloys using wire EDM to assess the surface integrity. Wire electric discharge machining yields better results than conventional procedures. Additionally, the pulse-on time factor emerged as the influential attribute for surface roughness and the MRR-material removal rate. Pramanik et al. (Ref 20) assessed the performance characteristics of WEDM on AA 6061 in terms of surface finish and material removal rate for various pulse-on time and wire tension. The assessment revealed that pulse-on time influences the material removal rate to a greater extent than does wire tension. A higher order of wire tension, on the other hand, facilitates better surface finish.

Swastik Kumar Kar et al. (Ref 21) carried out wire electric discharge machining of Inconel 625. The significant parameters contributing to the process were determined through a multi-objective optimization method. The experiments showed that the pulse-on time factor was the most significant, with a 64.14% contribution. Manoj and coworkers (Ref 22) observed the wire electrical discharge machining process characteristics of an austenitic nickel base alloy by adapting response surface methodology (RSM) and an artificial neural network (ANN). The results of the present study confirmed that the ANN approach is effective at assessing the output responses and errors, which constitute less than 6%.

Bineet Pal Singh et al. (Ref 23) investigated the machining performance of Nimonic-80A in the wire EDM process. The parameters were optimized using RSM. The analysis revealed that the peak current is the significant factor influencing the MRR and kerf width. Ravindra Bobbili et al. (Ref 24) presented the significance of WEDM parameters on the MRR and surface finish for armor steel. An L_{27} orthogonal array was developed to investigate this process. The investigation revealed that the pulse-on time and pulse-off factor significantly influence the roughness and MRR.

The above studies provide noteworthy insights into the process attributes of the WEDM process and the consequential effects on the characteristics of machined surfaces. The referenced literature survey furnishes extensive data on the machining of various grade steels: titanium-, hastelloy-, nimonic-, inconel-, aluminum- and hafnium-based alloys. Several studies have also contributed to highlighting the performance of stellite alloys processed through turning and milling. However, studies on the machining of stellite grade 6 B alloys through an EDM process integrated with approaches such as ANOVA, GRA and fuzzy logic systems for optimizing a set of parameters are rarely reported. The microstructure featuring a recast layer of machined stellite alloy with a high MRR and low Ra, as determined via elemental spectrum analysis, was also found to be sparse.

Henceforth, the comprehensive purpose of the present work is to fill this research gap by studying the machining characteristics of stellite-6B alloys. The behavior of the input attributes, such as pulse-on time, pulse-off time, wire feed, peak current and bed speed, at three sequential levels on machined stellite-6B alloys draws the attention of the authors to perform a parametric study. A package consisting of Taguchi analysis of variance, GRA (grey relation analysis) and a fuzzy logic system is used to regulate the process parameters at the optimal measurement for attaining a higher order of MRR and surface finish of the machined surface (i.e., a decreasing trend). The evaluation of 27 machined samples was conducted using a Taguchi orthogonal array. The optimization of the strategy with a statistical methodology enabled the accomplishment of the intended outcomes. The signal-to-noise ratio (S/N) and the mean derived from the analysis were used for parameter evaluation.

Optimal utilization of the WEDM capability requires appropriate selection of machining parameters. The present research also contemplates the necessity of establishing a scheme for multi-objective optimization. The accomplishment of this scheme involves defining appropriate measures of performance, developing a mathematical model, predicting the machining performance by selecting a proper optimization approach and applying this approach to a mathematical model to determine the combination of input attributes culminating in superior machining performance. The microstructural characteristics of the machined samples were also investigated and reported in the present work. This study also provides insight into the hardness profile of the machined samples. Furthermore, the fuzzy logic concept, which combines the surface roughness and material removal rate into a single variable, is used to determine the best combination of process parameters to improve the process.

2. Experimentation

2.1 Material Machining and Assessment Strategy

The base material chosen for the performance assessment was stellite 6B, a versatile and highly durable alloy primarily composed of cobalt, chromium, tungsten, nickel and molybdenum that contributed 63.40%, 29.10%, 3.61%, 1.10% and 0.29%, respectively**.** Stellite refers to alloys containing chromium and is designed to be resistant to galling, wear and corrosion. These alloys retain their properties at higher temperatures. Stellite, a cobalt-based alloy, consists of complex carbides in an alloy matrix. Experiments were carried out via CNC WEDM [SODIC JAPAN MODEL MARK 21 A500 W]. A brass wire of short diameter 0.25 mm was used as an electrode to cut a tiny kerf in the workpiece and the dielectric medium used for the process was deionized water.

A wire-cut EDM contains a machine tool with a flushing unit and a power supply. Wire movement is regulated from the top and lower wire guides through the work piece. The wire proceeds/advances through the commended path, and material separation from the workpiece occurs. A sequence of electric discharges (sparks) is induced between a precisely positioned movable wire and a workpiece machine for the materials in wire EDM. Through a dielectric medium, high-frequency alternating current pulses are discharged through a wire to an object piece with a very narrow spark gap. Multiple sparks can be observed at once. This is because genuine discharges can

occur up to 100,000 times every second, with discharge sparkles lasting only 1/millionth of a second or less. The needed surface finish and the intended cutting speed determine how much metal is removed during this brief spark discharge. A minute amount of material that is melted and evaporated from the object (workpiece) is removed by the heat generated by every electrical spark, which is estimated to be between 15,000° and 21,000° Fahrenheit. Through both the upper and bottom flushing nozzles, a stream of deionized/purified water is directed toward the chips and flushed away from the cut. The water also keeps the work item from overheating. The experimental view and assessment strategy used in the present study are shown in Fig. 1(a) and (b).

The pulse-on time determines the energy input during each pulse, affecting the material removal rate, surface finish and heat generation. The pulse-off time allows the machining zone to cool, reducing the thermal stress on the workpiece. The wire feed rate influences the cutting speed and accuracy. The peak current influences the intensity of the electrical discharge and, consequently, the material removal rate. The bed speed determines the rate at which the material is exposed to electrical discharge. Based on the available machine varying parameter settings and initial trial runs to fix the parameter level, the working parameters and their appropriate levels were selected, as indicated in Table 1.

2.2 Taguchi ANOVA and GRA

The study focused on the experiments performed under a full factorial design. The orthogonal array produces as few tests as possible in which a particular combination of different levels for a parameter is not tested again. Machinability performance was recorded via 27 experiments. The output responses from each unique set of experiments were inspected for the material removal rate (MRR), surface roughness (Ra) and grey relation grade (GRG). A MITUTOYO roughness meter was used to measure the surface roughness. The following equation is used to calculate the MRR:

$$\mathrm{MRR} = \frac{\text{Volume of the material removed}}{\text{Time taken}} \ \mathrm{mm^3/min} \quad (\text{Eq } 1)$$

From the experimentation, a factorial design was used for five dominant factors, namely the pulse-on time, pulse-off, wire

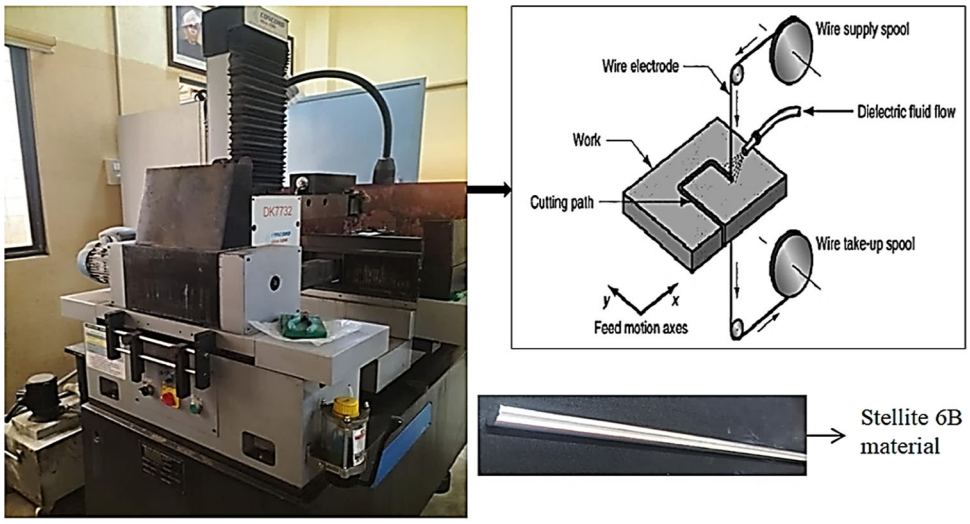

(a)

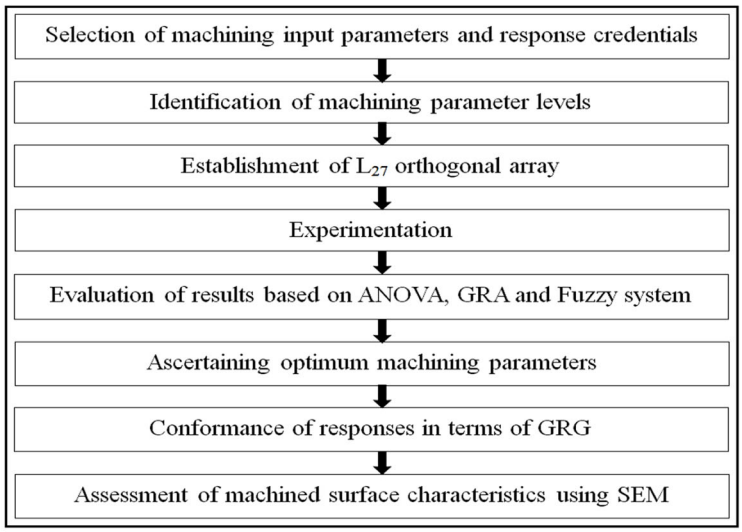

(b)

Fig 1 (a) Experimental view of the machining process and (b) Assessment strategy

Table 1 Working parameters and their levels

Sl no.	Process parameter		Levels		Reason for selecting the level
1	Pulse on, μs	40	60	80	Based on initial trial run
2	Pulse off, μs	10	15	20	Based on initial trial run
3	Wire feed, m/min	1	2	3	Range available in the machine
4	Peak current, A	3	4	5	Range available in the machine
5	Bed speed, μm/s	20	40	60	Range available in the machine

Table 2 L_{27} array with working parameters and responses

RUN	Pulse on, μs	Pulse off, μs	Wire feed, m/min	Peak current, A	Bed speed, μm /sec	MRR, mm^3/min	Ra, μm
1	40	15	1	4	60	10.2900	5.775
2	40	15	1	4	20	13.2860	5.558
3	40	15	1	4	40	9.8200	3.962
4	40	10	2	3	60	11.2220	3.925
5	40	10	2	3	20	10.8030	3.768
6	40	10	2	3	40	9.3600	4.068
7	40	20	3	5	60	12.4020	4.287
8	40	20	3	5	20	13.7600	3.981
9	40	20	3	5	40	14.7420	3.561
10	60	15	2	5	60	13.7610	4.399
11	60	15	2	5	20	10.4650	4.277
12	60	15	2	5	40	18.5120	3.633
13	60	10	3	4	60	9.6050	2.913
14	60	10	3	4	20	14.4950	5.084
15	60	10	3	4	40	9.3800	3.609
16	60	20	1	3	60	9.9100	4.463
17	60	20	1	3	20	15.0100	4.390
18	60	20	1	3	40	10.9800	4.886
19	80	15	3	3	60	9.8880	3.297
20	80	15	3	3	20	16.0810	4.401
21	80	15	3	3	40	18.0210	3.785
22	80	10	1	5	60	12.2220	3.753
23	80	10	1	5	20	18.2520	5.476
24	80	10	1	5	40	16.2865	5.535
25	80	20	2	4	60	13.2220	4.087
26	80	20	2	4	20	21.4100	4.930
27	80	20	2	4	40	15.4050	5.761

feed rate, peak current and bed speed contribution. The relationships between individual process parameters and each response were studied using the MINITAB application. For comparison and inference, the interaction between individual process attributes and associated consequences is strategized in the form of a contour plot. The set of control input parameters was optimized to a smaller scope of working entities through comprehended literature surveys, trial runs and expert knowledge. Based on the machine settings, certain ranges were chosen. Following the above sequence, the operating parameters suitable for machining stellite 6 'B' alloy were considered, and a set of processing attributes and their levels were provided. Table 2 displays the input parameters list with the output responses. The machined specimens are illustrated in Fig. 2.

The signal-to-noise ratio (S/N) and grey normalization values are computed based on the concepts of 'larger the better' and 'smaller the better' for surface roughness. A higher MRR is preferred since it denotes a faster rate of material removal. More material being removed per unit of time is implied by a higher MRR, which is generally regarded as beneficial in machining operations. The irregularities on the machined surface are measured in terms of surface roughness. A machined surface that is smoother and more refined is indicated by a lower surface roughness. The following equations illustrate the calculation of the S/N ratio:

$$\text{Larger, the better; } \frac{S}{N} = -10\log\left\{\frac{1}{n}\sum_{i=1}^{n} 1/y_i^2\right\} \quad \text{(Eq 2)}$$

$$\text{Smaller, the better; } \frac{S}{N} = -10\log\left\{\frac{1}{n}\sum_{i=1}^{n} y_i^2\right\} \quad \text{(Eq 3)}$$

where Y = responses for the given factor-level combination and n = number of responses in the factor-level combination.

Analysis of variance (ANOVA) is a key method for statistical analysis since it allows for simultaneous testing. By determining the most important element influencing the MRR

and surface roughness, ANOVA was used to verify the statistical validity of the model. The machining inputs and outputs are optimized using this method. Following Taguchi ANOVA, grey relation analysis is performed as a quantitative approach to observe the influence of each machining characteristic on the combined output responses, thereby improving the responses simultaneously. This analysis is primarily found in grey system theory and is used to analyze the relationships between systems, especially in cases with uncertain or limited information. It is necessary to normalize the experimental results of the MRR and Ra before using a GRA and fuzzy logic technique since their ranges are different. The equations for computing grey normalized values are as follows:

$$\text{Larger, the better; } x_i^*(k) = \frac{x_i^0(k) - \min x_i^o(k)}{\max x_i^0(k) - \min x_i^0(k)} \quad \text{(Eq 4)}$$

$$\text{Smaller, the better; } x_i^*(k) = \frac{\max x_i^0(k) - x_i^0(k)}{\max x_i^0(k) - \min x_i^0(k)} \quad \text{(Eq 5)}$$

where $x_i^*(k)$ indicates the normalized MRR or Ra for every run number 'k' and $x_i^0(k)$ refers to the MRR or Ra for run number 'k'.

The grey relation coefficient (GRC) is computed by the equation below:

$$\zeta_i^*(k) = \frac{\Delta_{\min} + \zeta * \Delta_{\max}}{\Delta_{0i}(k) + \zeta * \Delta_{\max}} \quad \text{(Eq 6)}$$

where $\zeta_i^*(k)$ represents the grey relational coefficient and Δ_{min} and Δ_{max} are the minimum and maximum deviations, respectively. 'ζ' refers to the distinguishing coefficient, and its value is 0.5.

The GRG is attained by considering the average values of the GRC. Table 3 shows the tabulated and presented sets of grey normalized values, deviation sequence values, GRC and GRG for the output responses.

3. Results and Discussion

3.1 Statistical Analysis

The experiments were performed in accordance with the L_{27} orthogonal array to explore the credibility of the input attributes on the desired output performance characteristics in WEDM machining of stellite-6B alloys. The optimum process parameters were ascertained to determine the effective and efficient machining process. A higher MRR and GRG and a lower Ra were the indices used to indicate superior performance. The quadratic regression model proposed to predict the MRR, Ra and GRG is expressed as a function of the working parameters in Eqs. 7, 8 and 9:

$$\begin{aligned}\text{MRR} &= 3.84 + 0.0975 * (\text{Pulse On}) + (0.169) * (\text{Pulse Off}) \\ &\quad + (0.129) * (\text{Wire feed}) + (1.063) \\ &\quad * (\text{Peak current}) - (0.0862) * (\text{Bed speed})\end{aligned} \quad \text{(Eq 7)}$$

$$\begin{aligned}\text{Ra} &= 4.74 + (0.00594) * (\text{Pulse On}) + (0.0246) \\ &\quad * (\text{Pulse Off}) - (0.493) * (\text{Wire feed}) + (0.107) \\ &\quad * (\text{Peak current}) - (0.01379) * (\text{Bed speed})\end{aligned} \quad \text{(Eq 8)}$$

Fig 2 The machined specimens

$$\begin{aligned}\text{GRG} &= 0.258 + (0.001806) * (\text{Pulse On}) - (0.00022) \\ &\quad * (\text{Pulse Off}) + (0.0506) * (\text{Wire feed}) + (0.0100) \\ &\quad * (\text{Peak current}) - (0.000194) * (\text{Bed speed})\end{aligned} \quad \text{(Eq 9)}$$

This section highlights the experimental campaign of the parametric influences on the machining characteristics and the optimization of parameters. Figure 3 (a), (b) and (c) represents the residual plots for MRR, Ra and GRG, respectively, obtained from 27 experimental runs. The plots demonstrate that independent residues display random dispersion. Furthermore, the variable follows a normal distribution, while the residuals are roughly distributed in a straight line, exhibiting an appreciable liaison analytically between the predicted values for all output performances and the experimental results.

ANOVA was employed to assess the effect of each input parameter on the response variables MRR, Ra and GRG. Tables 4, 5 and 6 show the response details for the S/N ratio on the MRR, Ra and GRG of the stellite−6B alloy. The combined response table reveals that the wire feed is the working parameter that has the most influence on the GRG, followed by the pulse-on factor, peak current, bed speed and pulse-off.

3.2 Parameter Influence on the MRR

The response of the MRR to variations in process parameters in the form of contour plots is illustrated in Fig. 4 (a-c).

Pulsing is the duration of time needed for the impingement of an electrical spark on a workpiece because the material melts. Pulse generators provide the necessary spark energy at the required intervals (Ref 25). The spark will have all the required energy and is made available as soon as the gap conditions are right for sparking. To initiate electrical discharge and generate pulses, the power supply sends a series of short controlled electrical pulses to the wire electrode. These pulses create a high-intensity electric field within the spark gap. When the voltage across the spark gap reaches a critical point, ionization of the dielectric fluid occurs, thereby creating a

Table 3 Grey relation analysis

	Grey normalized values		Deviation sequence values		Grey relation coefficient		
RUN	MRR, mm^3/min	Ra, μm	MRR, mm^3/min	Ra, μm	MRR, mm^3/min	Ra, μm	GRG
1	0.08	0.00	0.92	1.00	0.35	0.33	0.34
2	0.33	0.08	0.67	0.92	0.43	0.35	0.39
3	0.04	0.63	0.96	0.37	0.34	0.58	0.46
4	0.15	0.65	0.85	0.35	0.37	0.59	0.48
5	0.12	0.70	0.88	0.30	0.36	0.63	0.49
6	0.00	0.60	1.00	0.40	0.33	0.55	0.44
7	0.25	0.52	0.75	0.48	0.40	0.51	0.46
8	0.37	0.63	0.63	0.37	0.44	0.57	0.51
9	0.45	0.77	0.55	0.23	0.47	0.69	0.58
10	0.37	0.48	0.63	0.52	0.44	0.49	0.47
11	0.09	0.52	0.91	0.48	0.36	0.51	0.43
12	0.76	0.75	0.24	0.25	0.68	0.67	0.67
13	0.02	1.00	0.98	0.00	0.34	1.00	0.67
14	0.43	0.24	0.57	0.76	0.47	0.40	0.43
15	0.00	0.76	1.00	0.24	0.33	0.67	0.50
16	0.05	0.46	0.95	0.54	0.34	0.48	0.41
17	0.47	0.48	0.53	0.52	0.48	0.49	0.49
18	0.13	0.31	0.87	0.69	0.37	0.42	0.39
19	0.04	0.87	0.96	0.13	0.34	0.79	0.57
20	0.56	0.48	0.44	0.52	0.53	0.49	0.51
21	0.72	0.70	0.28	0.30	0.64	0.62	0.63
22	0.24	0.71	0.76	0.29	0.40	0.63	0.51
23	0.74	0.10	0.26	0.90	0.66	0.36	0.51
24	0.57	0.08	0.43	0.92	0.54	0.35	0.45
25	0.32	0.59	0.68	0.41	0.42	0.55	0.49
26	1.00	0.30	0.00	0.70	1.00	0.42	0.71
27	0.50	0.00	0.50	1.00	0.50	0.33	0.42

conductive plasma channel. Ionization initiates a spark or electrical discharge at the wire–work piece juncture.

From Fig. 4(a), with a higher pulse-on factor, the energy residing in the plasma channel is high, resulting in high temperature and pressure within the plasma channel. With an increase in the pulse-on factor electrons, the surface per discharge/transfer of thermal energy to the surface increases, resulting in the erosion of the material (Ref 26). The material removal rate shows an increasing trend with increasing pulse-on time because the amount of thermal energy that is transferred to the workpiece surface increases, causing more material to melt. Increased discharge energy and pulse-on time lead to improved cutting speed, contributing to high MRR.

The increase in the MRR with respect to pulse-on time can also be attributed to the fact that with increasing time, the discharge electric sparks tend to increase, and these high-intensity electric sparks tend to deepen the cut on the workpiece and thereby increase the MRR. Additionally, heat generated during pulse-on time widens the heat-affected zone of the workpiece, producing possible craters during the subsequent cycle (Ref 9).

A higher peak current during machining results in a surpassing discharge between the workpiece and wire electrode, culminating in an MRR of higher magnitude. At higher values, a higher discharge energy density contributes to increased temperature; therefore, more melting of the metal occurs, consequently enhancing the material removal rate. As the peak current increases, the cutting speed also tends to increase because the wire electrode moves through the workpiece material more quickly, resulting in a higher MRR.

An ionization channel at the proximity of the wire to the workpiece is established at the initiation of the process. The actual discharge process continues to occur at higher current intensities. Ionization of the channel occurs with a heavy flow of current, creating a magnetic field and compressing the ionization chamber. As the temperature increases, melting and vaporization progress, leading to erosion of the wire and workpiece (Ref 27).

Longer pulse-off time typically results in shorter intervals between effective machining pulses, and servo voltage could slightly widen the working gap between the electrode and workpiece, which lowers the MRR (Ref 28). The pulse-off duration is the time when the dielectric was deionized. An inadequate time might cause unpredictable cycling and retraction of the advancing servo, slowing the operating cycle and resulting in a decrease in the MRR with increasing pulse-off.

The period of time when capacitors discharge without causing a spark is referred to as the pulse-off. The deionization of dielectric fluid also occurs during this interval, implying that machining does not occur during this time. As a result, increasing the pulse off lengthens the cycle while decreasing the spark frequency, resulting in a reduction in the MRR (Ref 29). The pulse-off time is the time for two consecutive sparks when no current is supplied to the electrode. As a result, the MRR will drop.

The pulse-off duration is the time period (μs) between sparks. The temporal interval separates two pulses in a single time period. There is no machining during the pulse-off time (idle time interval), which allows the melted material to evaporate and eliminate debris from the machining area. This

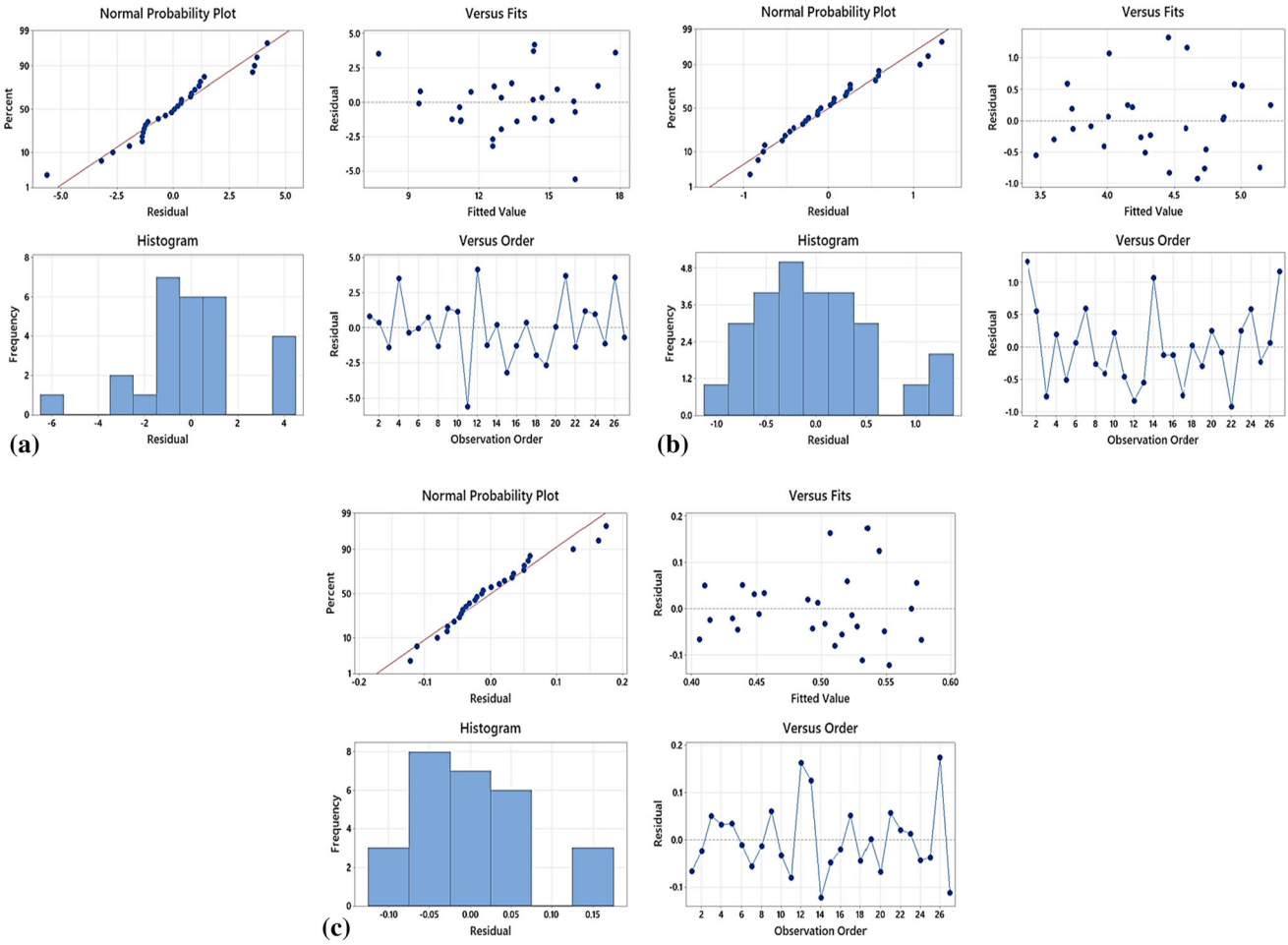

Fig 3 Residual plots for (a) MRR, (b) Ra, and (c) GRG

Table 4 Response of the S/N ratio to the MRR

Level	Pulse-on, μs	Pulse off, μs	Wire feed, m/min	Peak current, A	Bed speed, μm/s
1	21.30	21.62	22.00	21.61	23.22
2	21.68	22.25	22.49	21.96	22.37
3	23.68	22.79	22.16	23.08	21.06
Delta	2.39	1.16	0.49	1.47	2.17
Rank	1	4	5	3	2

Table 5 Response of the S/N ratio to Ra

Level	Pulse on, μs	Pulse off, μs	Wire feed, m/min	Peak current, A	Bed speed, μm/s
1	−12.59	−12.36	−13.65	−12.22	−13.28
2	−12.32	−12.62	−12.62	−13.10	−12.55
3	−13.02	−12.95	−11.67	−12.61	−12.11
Delta	0.70	0.59	1.98	0.88	1.17
Rank	4	5	1	3	2

parameter influences the machining rate and cut stability, thereby reducing the order of the MRR (Ref 30), as shown in Fig. 4(b).

With increasing pulse-off time, there is a decreasing trend in the MRR with decreasing amplitude of variation. This is attributed to the fact that the number of discharges inside the

Table 6 Response of the S/N ratio to the GRG

Level	Pulse on, μs	Pulse off, μs	Wire feed, m/min	Peak current, A	Bed speed, μm/s
1	−6.813	−6.129	−7.227	−6.285	−6.195
2	−6.257	−6.267	−5.975	−6.426	−6.085
3	−5.565	−6.239	−5.433	−5.925	−6.355
Delta	1.249	0.138	1.794	0.501	0.270
Rank	2	5	1	3	4

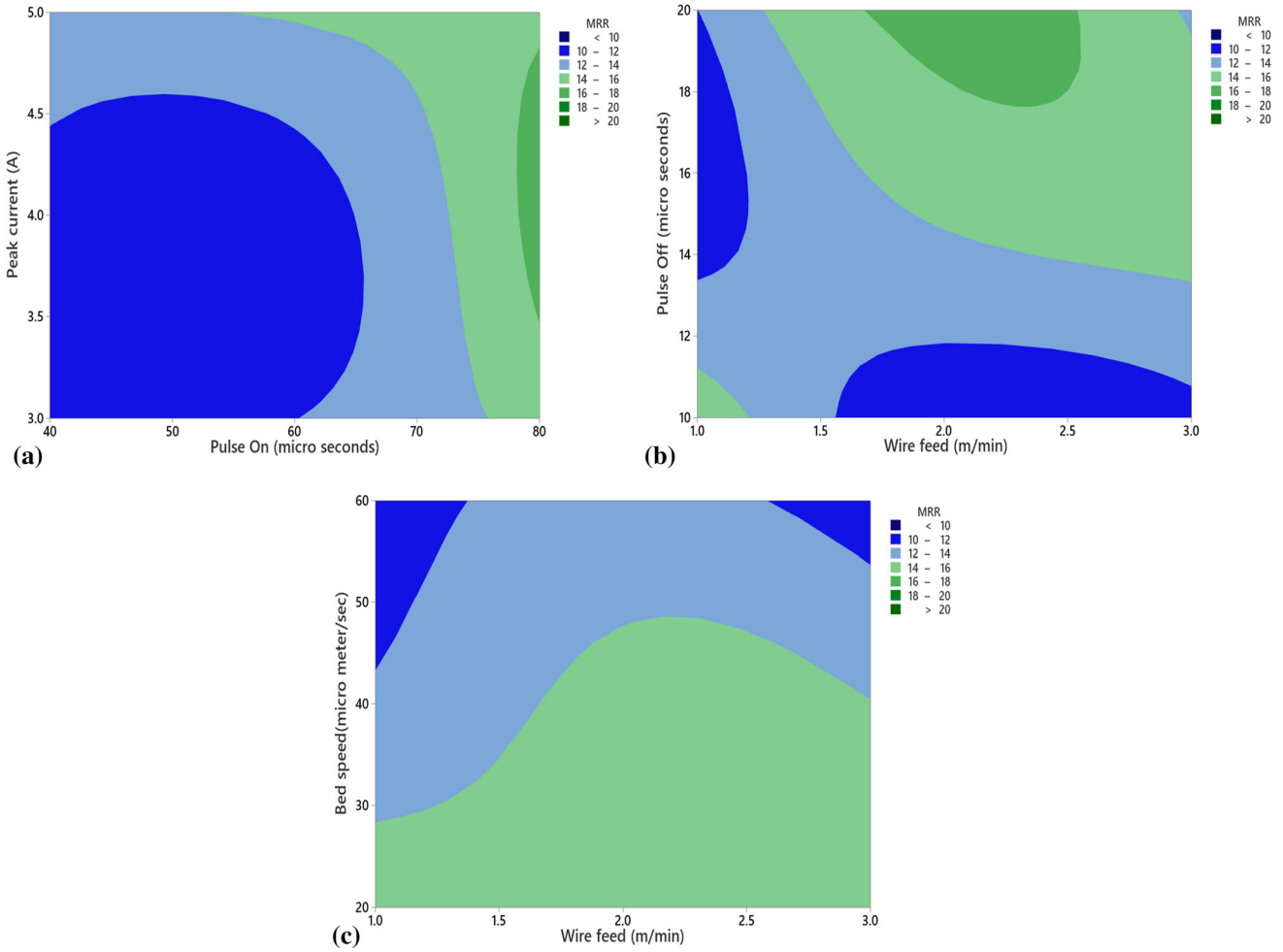

Fig 4 Contour plots for the MRR

intended time interval decreases as the interval between the two pulses increases, leading to a decrease in the cutting speed. Following this, there may be a reduction in the plasma channel melt rate and ignition of sparks ratio, annihilating the MRR (Ref 31).

WEDM aids in transforming electrical energy to thermal energy, which is utilized for cutting materials. An increased wire feed rate allows faster or easier access to new wire surfaces, resulting in more sparks and, ultimately, improved material removal. The MRR initially decreases as a result of consumed or degraded wire. With an increase in wire feed, marginal improvement is observed. Effective sparks are produced as a result of quickly replacing eroded wire with new wire, accelerating the material removal rate (Ref 32, 33).

The bed speed determines how quickly the wire electrode progresses through the workpiece material, affecting the material removal rate and overall machining efficiency. An increase in bed speed usually leads to a higher MRR, as shown in Fig. 4(c). This is because wire electrodes moving at a faster pace can erode material more quickly. As the wire electrode moves faster, more heat is generated due to the increased electrical discharge energy. This can aid in melting and vaporizing the workpiece material more efficiently (Ref 34).

3.3 Parameter Influence on Ra

The response of the surface roughness, Ra, to the variation in process parameters in the form of contour plots is illustrated in Fig. 5(a-c).

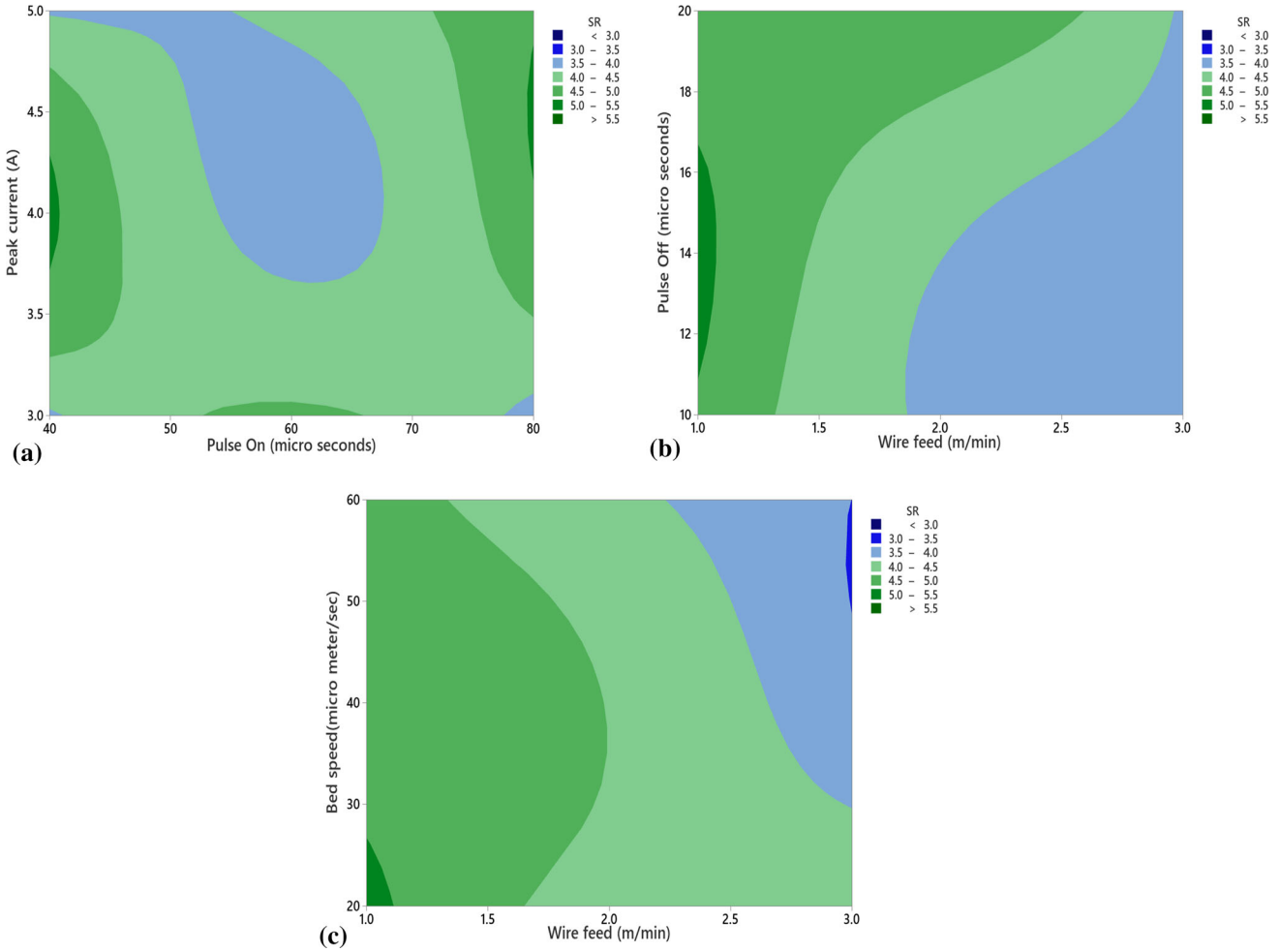

Fig 5 Contour plots for Ra

The consequence of the pulse-on factor on the surface roughness is depicted in Fig. 5(a). The heat-affected zone is widened by the sparking effect, and debris on the surface is flushed away to a minimal extent with dielectric fluid. This could also explain the decrease in the surface finish (Ref 35). Surface roughness varies in proportion to pulse-on time. An increase in pulsing on and energy discharge results in enlarged channels. Intense heat from the spark leads to possible formation of craters owing to work piece melting followed by vaporization, thereby increasing Ra (Ref 36, 37).

An increase in the pulse-on time increases the heat-affected portion of the specimen, resulting in melting of the stellite in a disproportionate fashion/trend and leading to the formation of cracks, reducing the surface integrity of the machined surface. With a higher order of pulse-on time during the process, the electric sparks persist for a long time, leading to the expulsion of the melt from the alloy; therefore, the integrity is affected.

From Fig. 5(b), the maximum roughness prevails at a lower order of pulse-off time. With an extended pulse-off factor, material melting and evaporation depend mainly on the discharge energy. Fewer discharges occur in a given time, in addition to dielectric media assisting in flushing/sweeping away the eroded substance, thereby resulting in a marginal reduction in Ra (Ref 38, 39).

With increasing pulse-off time, the surface roughness of the machined surface tended to decrease. This could be ascribed to the fact that as the pulse-off time increases, the flushing time of the dielectric fluid also tends to increase, which flushes away the debris and molten expulsion to a greater extent to achieve a clean surface. The flushing of dielectric fluid helps increase the surface integrity of the sample specimen.

With increasing peak current, the discharge energy increases. Escalated discharge energy results in crater formation, leading to an inferior surface finish (Ref 40). A longer spark time indicates a longer residence time for discharge, leading to a high cutting speed and discharge energy, thereby deteriorating the surface finish (Ref 41). Ra increases with increasing peak current. A higher order of energy discharge on a workpiece results in the formation of voids and craters.

The surface roughness is more pronounced at lower wire feed ranges. A lower wire feed results in a reduction in the cutting speed. Under these conditions, a rough surface is generated owing to abrupt sparks developing uneven and overlapped craters on the surface. With an increase in the wire feed rate from 1 m/min to 3 m/min, the surface roughness tends to decrease. The decrease in Ra with respect to the wire feed rate is due to the high-intensity sparks discharged through the newly introduced wire surface during the process, resulting in a decrease in the surface roughness of the machined surface (Ref 9).

A higher bed speed can lead to increased material removal rates. However, at high speeds, the EDM process can become

less stable, potentially causing surface roughness due to increased discharge energy and higher heat input. This can result in a rougher surface finish. Slower bed speeds may offer more control over the EDM process, resulting in improved surface finish due to reduced discharge energy, as shown in Fig. 5(c). However, excessively low speeds might prolong the machining time, leading to increased tool wear and higher production costs.

3.4 Optimum Machining Parameters

The optimization of machining parameters in wire EDM is essential for achieving the best results in terms of accuracy, surface finish and efficiency. To optimize these parameters effectively, trials and experiments are often needed while considering the specific material, shape and tolerance requirements of the workpiece. Advanced software tools and the expertise of operators and machinists play a significant role in finding the ideal combination of settings for each unique machining task. The primary effects of the S/N ratio on MRR, Ra and GRG are plotted against all of the input parameters in Fig. 6(a), (b) and (c), respectively.

It is evident that the input factor slopes of the lines connecting data points of various levels vary. As a result, the various concentrations had distinct effects on the MRR, Ra and GRG. The level of the parameters for machining with the highest S/N ratio is regarded as the ideal level. Thus, for pulse-on, pulse-off factors, wire feed rate, peak current and bed speed, the highest MRRs are attained at 80 μs, 20 μs, 2 m/min, 5 A and 20 m/s, respectively. On the other hand, the lowest Ra is achievable at 60 μs, 10 μs, 3 m/min, 3 A and 60 μm/s. For combined responses, the highest GRG was reached at 80 μs, 10 μs, 3 m/min, 5 A and 40 μm/s.

3.5 Conformance of the Responses

The conformity of responses during wire EDM refers to the accuracy and consistency of the machining process in relation to the input commands or desired specifications. Achieving conformity in response is decisive for maintaining the quality and precision of machined parts. The relationships between various input parameters and the output performance in wire EDM are assessed through grey relational analysis. The grey relation grade is a measure of the relationship between a reference series and a comparison series. It is used to analyze the correlation or similarity between different factors or parameters in a system. The grey relation grade represents the relative significance of different input attributes based on the output performance criteria. Hence, the GRA technique is invoked to address the multiple performance characteristics of the WEDM process (Ref 42).

The optimum machining parameters for achieving higher GRGs were 80 μs, 10 μs, 3 m/min, 5 A and 40 μm/s. According to the quadratic regression model (Eq. 4), the predicted GRG at the optimum level of the machining parameters was 0.594, and the found experimental GRG was 0.489. Figure 7 shows the predicted and experimental GRGs.

The obtained error percentage among the outcomes was 17.67%. This observation may be associated with the inherent properties of stellite 6B material, which can lead to possible wire breakage/discontinuity during machining, inconsistent cutting rates, or difficulties in maintaining dimensional accuracy. The localized heat generated during the machining process might not dissipate effectively, leading to thermal stresses that could cause changes in material properties, affecting accuracy.

3.6 Fuzzy Logic Approach

Fuzzy logic is a heuristic approach that allows for more advanced decision-tree processing and better integration with rules-based programming. The concept of carrying out an optimization operation with many performance characteristics is used in regard to predicting the ideal combination of process parameters that attains the maximum MRR and minimum Ra jointly rather than for each parameter separately. With fuzzy logic, two input spaces can be mapped to a single output space while taking the combined MRR and SR as GRGs into account (Ref 43). Using the MATLAB application, an inference model of the Mamdani type is constructed and is shown in Fig. 8.

The grey relation coefficients of MRR and Ra are the inputs for the inference system in each experiment, and the outcome is referred to as the fuzzy GRG. Every input encounters three triangle membership functions assigned to it, and the output possesses five triangular membership functions. To map the inputs to the output, nine 'If and then' fuzzy rules are used. Figure 9(a-c) illustrates the membership functions for the input and output variables.

Utilizing the centroid defuzzification technique, the input value is transformed into a fuzzy GRG. The designed inference model is shown in Fig. 10. Considering that run number 16 produces the highest Fuzzy GRG, a combination of process parameters, pulse-on time = 60 μs, pulse-off = 20 μs, wire feed rate = 1 m/min, peak current = 3 A and bed speed = 60 μm/s, can be proposed.

The relationship between a GRG and a fuzzy GRG in wire EDM lies in the incorporation of fuzzy logic to handle the inherent uncertainties in the machining process. Fuzzy GRG provides a more flexible and adaptable approach, allowing for the consideration of imprecise or ambiguous information in the evaluation of machining parameters and their impact on performance. GRGs and fuzzy GRGs are tools used in systems analysis, and extension to the fuzzy domain makes fuzzy GRGs particularly useful when dealing with uncertainties or imprecise information in the context of wire EDM. The variations in the GRG and fuzzy GRG according to the present study and the primary effects of the S/N ratio on fuzzy GRG are displayed in Fig. 11(a) and (b). Table 7 shows the optimum levels of the parameters determined via ANOVA.

3.7 Machined Surface Characteristics using SEM

A microstructural investigation of the machined surface was carried out to assess the characteristics of the surface machined during WEDM. The samples were etched with aqua regia solution and examined using optical and scanning electron microscopy (OM and SEM) techniques. Energy dispersion spectroscopy (EDS) reveals the elemental constituents of the machined alloy surface. With higher discharge energy, the MRR is pronounced, leading to the formation of wider craters. Since wire EDM employs thermal energy, the machining zone counteracts a high temperature gradient due to heating and simultaneous quenching effects from the dielectric medium. As a result, the materials that are melted are resolidified on the outer surface of the specimen. This layer is termed the recast layer (Ref 44).

The SEM images illustrated in this section show the recast layer formed on the machined surface for the highest and

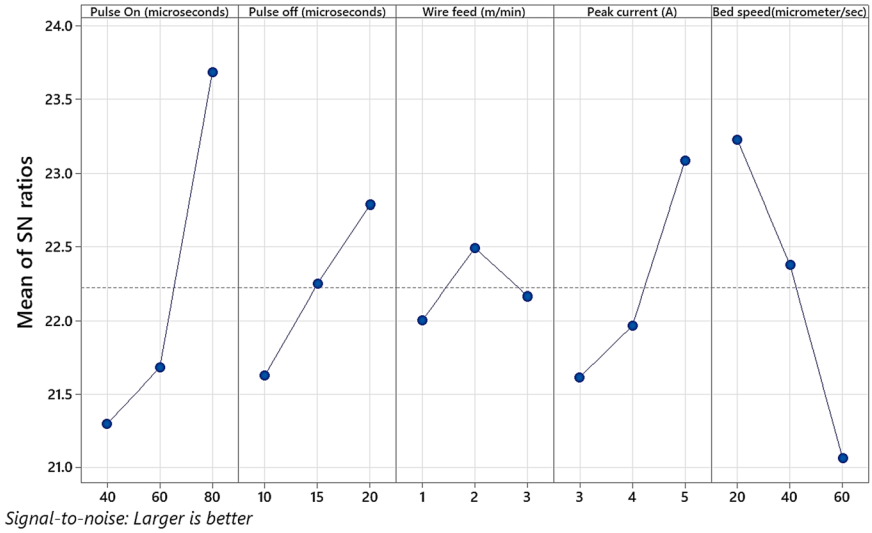

(a)

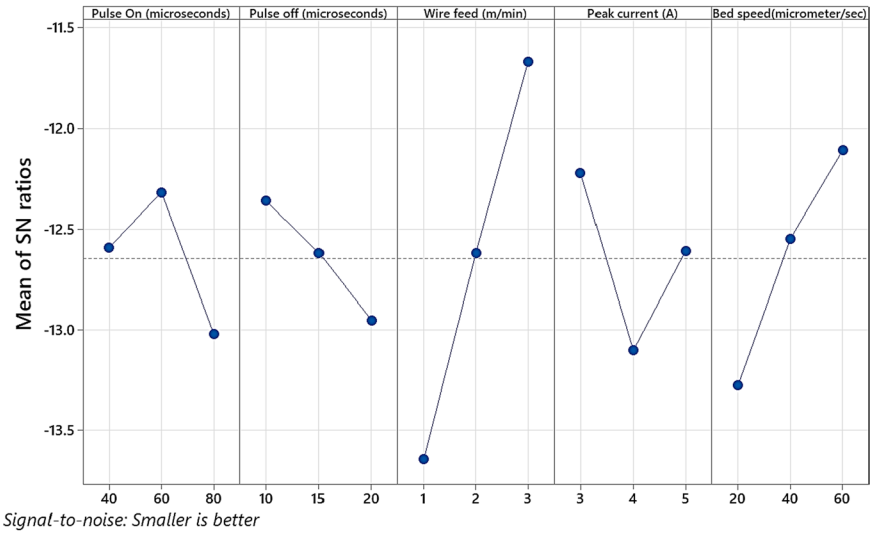

(b)

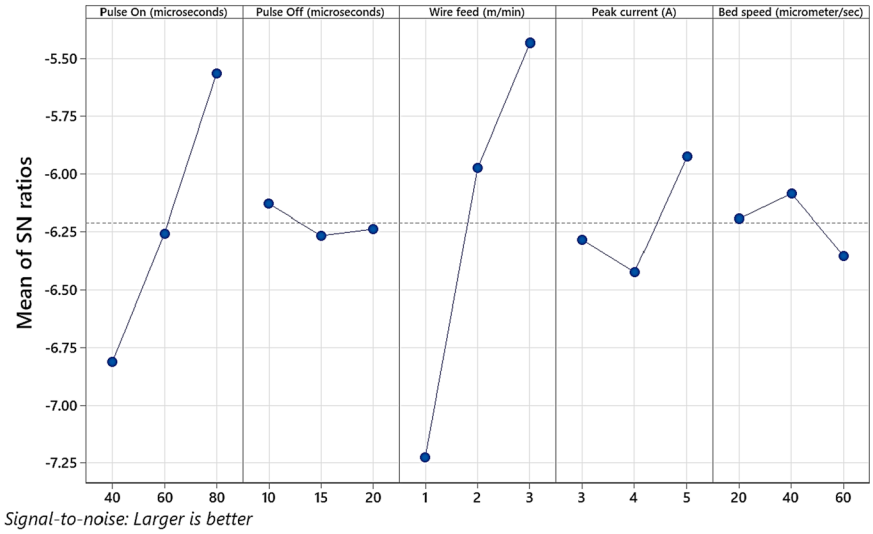

(c)

Fig 6 Primary effects plot for S/N ratios on (a) MRR, (b) Ra and (c) GRG

lowest machining responses. The recast layer is a white layer that forms when heat develops during WEDM because the molten material cools and hardens on the surface. This fragile layer is prone to failure and changes the dimension and shape of the machined parts (Ref 45). Figure 12(a-e) shows the evolution of the recast layer with a higher MRR of 21.41 mm^3/min and a moderate Ra of 4.93 μm.

Figure 12(a) and (b) shows the microstructure of the wire cut edge at 200× magnification and 500× magnification, respectively. The micrograph shows a very thin recast layer due to the wire-cut process. Thickness of the white layer in heat-affected zone, spark hardening and coarsening of the substrate are directly related to spark intensity. Additionally, the pulse discharge energy affects the thickness of the recast layer. When the energy of pulse discharge is high, the thickness of the recast layer is also more and vice versa. This is because higher discharge energies increase the net volume of the molten workpiece, which finally freezes and adheres to the machined surface due to rapid dielectric quenching (Ref 46). The recast layer is measured as less than approximately 10 microns. The optical microstructures along the metal matrix edges show that the carbides in the cobalt solid solution matrix are unaffected by chromium (Cr_7C_3 and $M_{23}C_{6,}$ which are intermetallic precipitates) and other heavy metal carbides. The alloy carbides are resolved with no recrystallized grains.

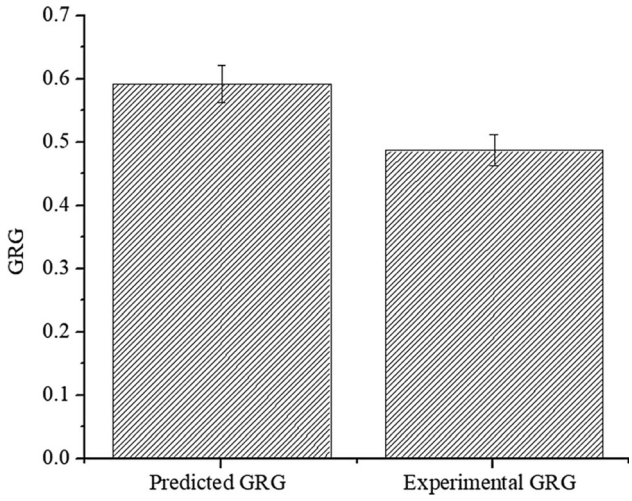

Fig. 7 Predicted and experimental GRG

The SEM image in Fig. 12(c) shows the recast layer along the edges of the sample. The thickness of the recast layer varies from 10 to 15 microns. The magnification is 500×. The inner base metal matrix shows the presence of fine voids along the edges and recast layer. The voids could also be melting voids. The parent metal grains are not significantly affected by the EDM process. From the SEM image in Fig. 12(d) at 2000×, the carbides formed are resolved because large grains do not seem to have undergone recrystallization due to the heat of the process.

The recast layer edge surface was selected for the evaluation of the elemental presence and quantity on the surface. As indicated in Fig. 12(e), the 'red' region was selected for energy dispersion spectroscopy because it shows the elemental constituent map of the machined surface. The weight percentages (%) of the detected elements from the base metal, namely carbon, oxygen, sodium, aluminum, chlorine, chromium, manganese, iron, cobalt, nickel and molybdenum are 6.17, 2.17, 1.31, 2, 1.04, 28.66, 1.49, 2.49, 50.52, 3.05 and 1.12, respectively. The high carbon content is due to the formation of multiple carbides of chromium. The high oxygen content is due to the oxidation of the edge during the wire-cutting process with atmospheric oxygen. The presence of oxygen and carbon could be attributed to the decomposition of the dielectric fluid at very high temperatures. With the increase in the spark energy, additional gas is generated by the evaporation of the dielectric fluid. This gas is then entrapped in the redeposited material, which results in microvoids and surface irregularities (Ref 47). The weight percentages (%) of cobalt and chromium in the recast layer are 50.52 and 28.66, respectively, which is comparatively lesser than the raw material. This reduction is due to induced heat, subsequent melting and material vaporization.

A recast layer formed on the machined surface with a lower Ra of 2.913 m and a 9.605 mm^3/min MRR, as depicted in Fig. 13(a-e).

Figure 13 (a) and (b) displays the microstructure of the wire cut edge at 200 and 500×, respectively. Because of the wire-cut operation, the micrograph displays an extremely thin recast layer. The recast layer is measured to be approximately 10 microns thick. The unaffected carbides of chromium (Cr_7C_3 and $M_{23}C_6$) and other heavy metal carbides in the cobalt solid solution matrix are visible in the microstructure along the metal matrix edges. The alloy carbides are resolved in Fig. 13(b).

The recast layer is visible at the sample margins in Fig. 13(c). The recast layer ranges in thickness from 15 to 20 microns. The precipitated alloy carbides of chromium in a

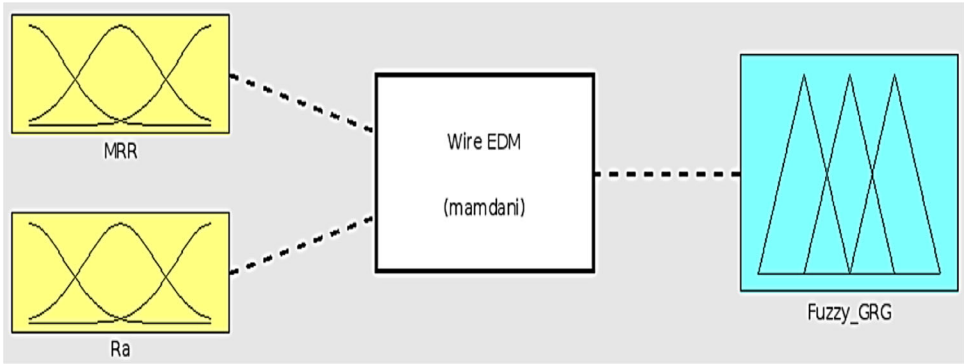

Fig. 8 Mamdani model

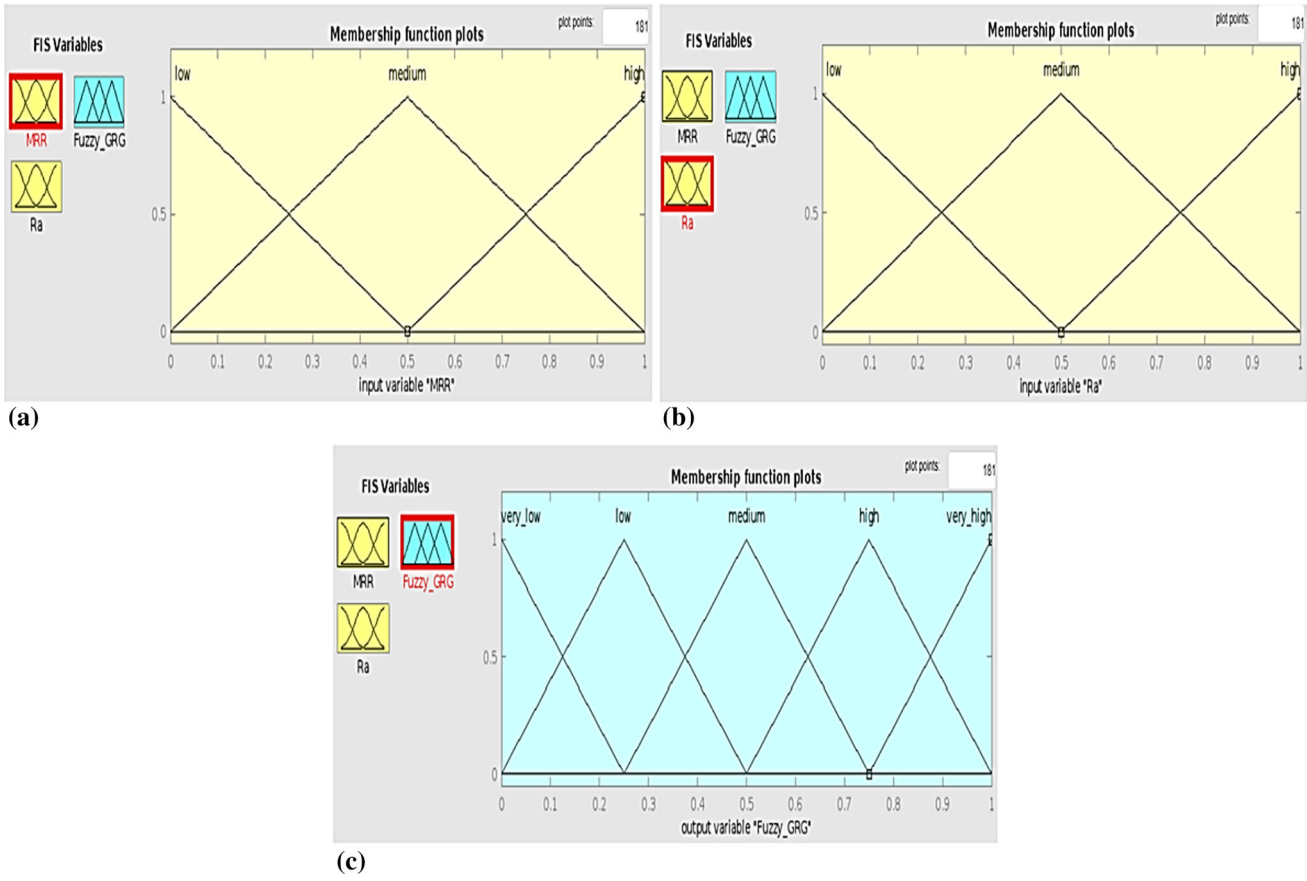

Fig. 9 Membership functions (a, b) input variables, (c) output variable

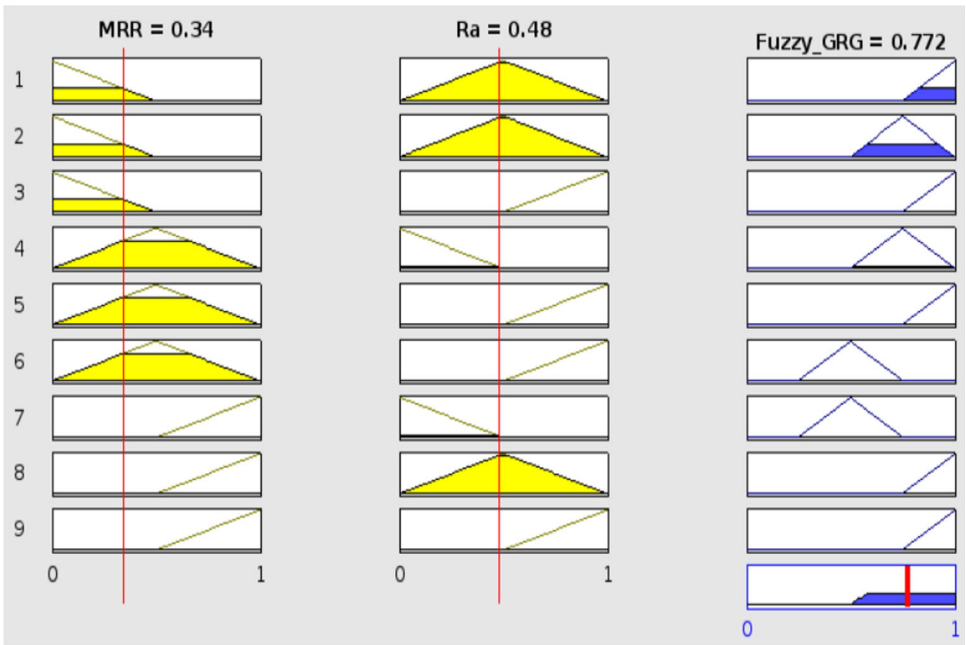

Fig. 10 Designed inference model

solid solution of base metal cobalt are visible in the inner matrix. Micropores can be observed along the recast layer under the microscope at 500×. At higher magnification, the recast layer stuck to the base metal. The boundaries of the recast layer are distinctly delineated. The large grains of alloy carbides are resolved. The examination of the SEM images revealed the formation of microcracks/micropores on the

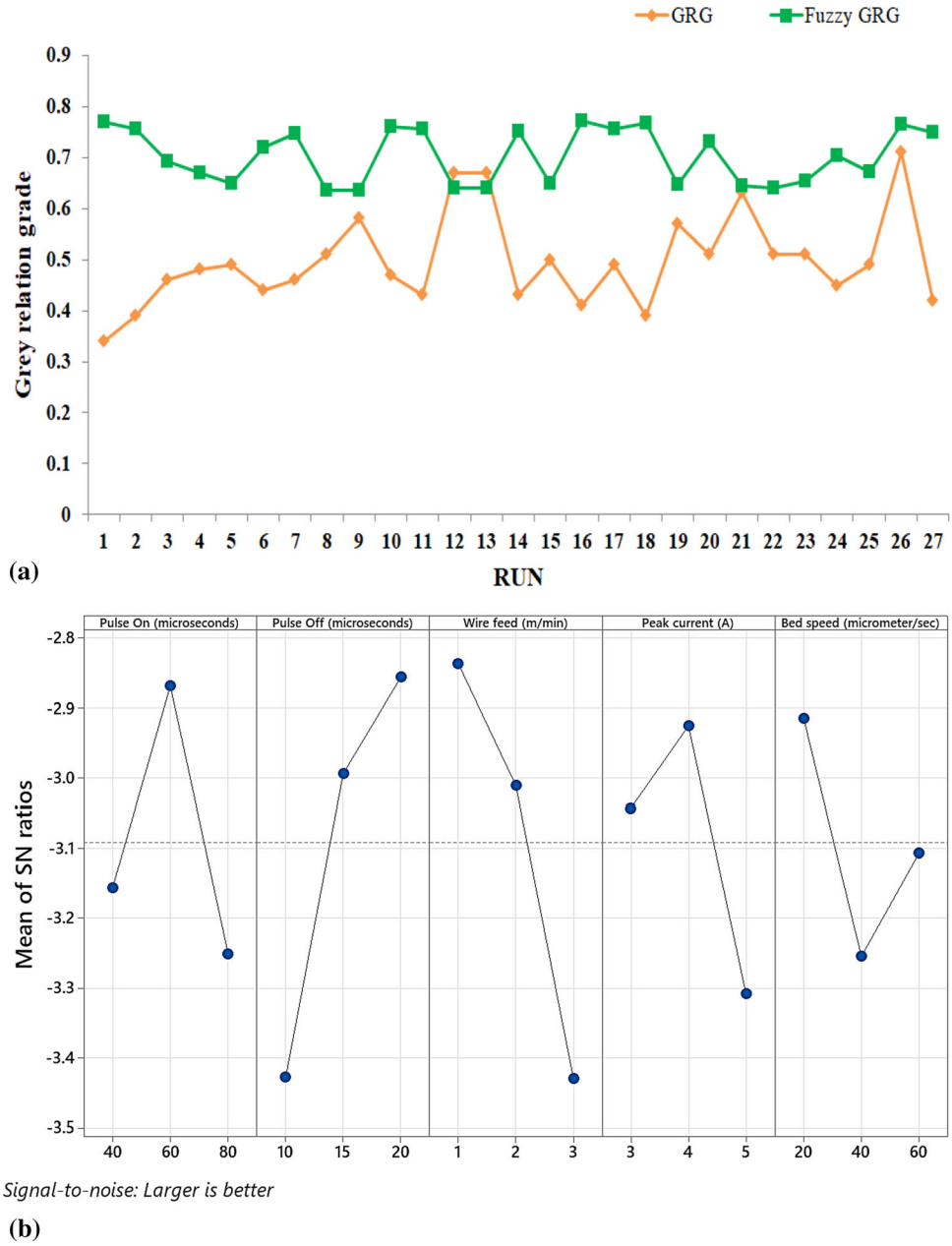

Fig. 11 (a) GRG and fuzzy GRG, (b) primary effects plot for S/N ratios on fuzzy GRG

Table 7 Optimum conditions from ANOVA

Responses	Pulse on , μs	Pulse off, μs	Wire feed, m/min	Peak current, A	Bed speed, μm/s
MRR	80	20	2	5	20
Ra	60	10	3	3	60
GRG	80	10	3	5	40
Fuzzy GRG	60	20	1	4	20

surface due to rapid solidification of molten material by means of dielectric fluid.

The inner edge of the wire cut edge is depicted in Fig. 13(d) together with the grain boundary gaps and massive alloy carbides (Cr_7C_3 and $M_{23}C_6$). During the EDM process, craters are formed. At 2000×, the carbides that develop are resolved as large grains and do not appear to have experienced recrystallization as a result of heat from the process. Material removal phenomena lead to crater formation. During the pulse-on time, the material never boils due to the overpressure of the plasma. When the discharge ends, the liquid medium's inertia causes the bubble to continue expanding, which causes a sudden drop in

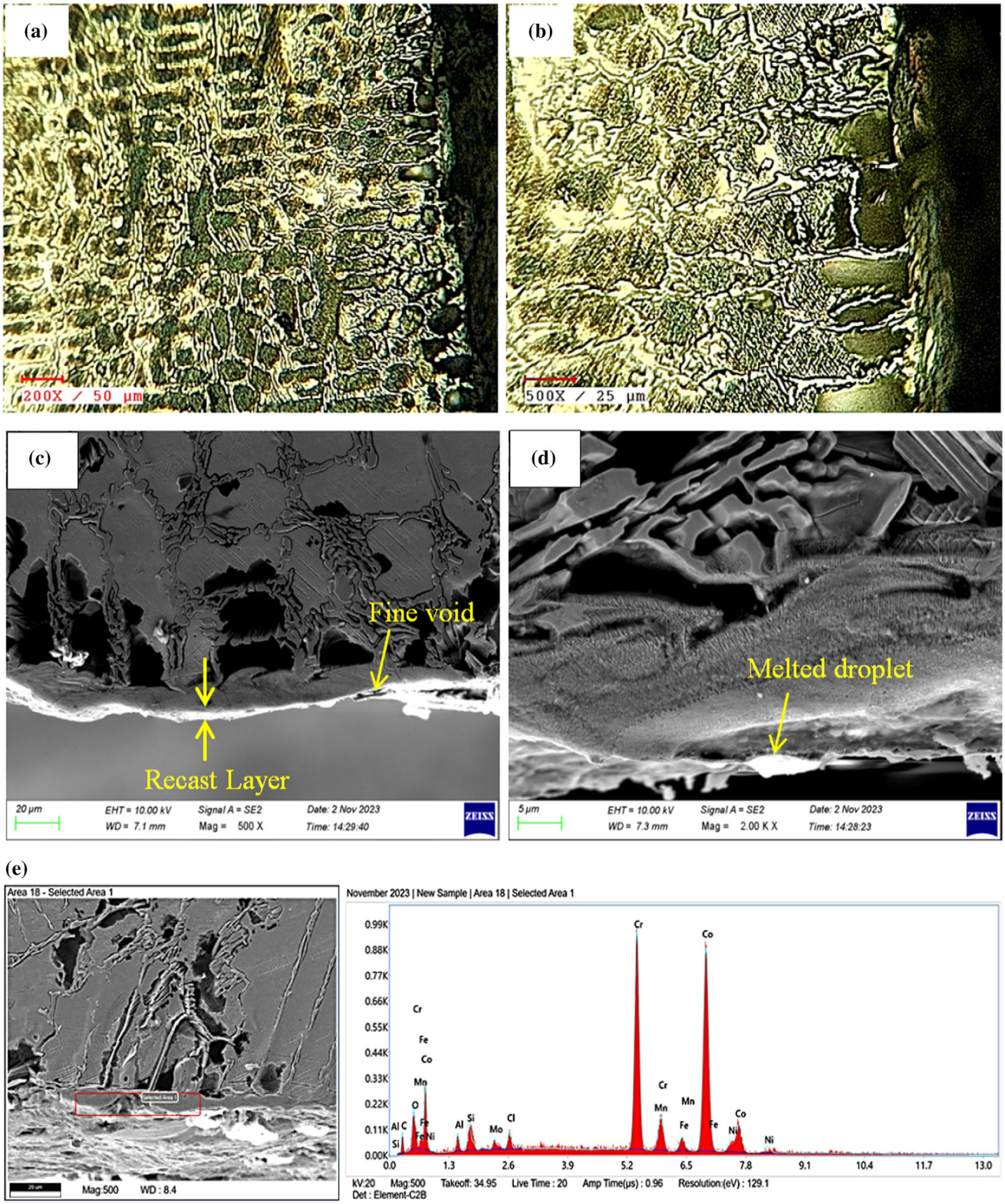

Fig. 12 (a, b) Optical micrographs, (c, d) SEM images, (e) edge surface EDS image

internal pressure and the creation of a local vacuum, which allows the molten metal from the crater to splash (Ref 48).

The core surface, as indicated in Fig. 13(e), was selected for the evaluation of the elemental presence and quantity on the surface. This field was selected for EDS observation. The constituents with 'K' shell elements detected were C (5.12%), O (1.85%), Cr (35.56%), Mn (1.27%), Fe (2.02%), Co (47.68%), Ni (2.4%) and W (4.09%). It is evident that the carbon content from the inner core is lower because the alloy carbides are from the base metal and low oxygen content during the EDM process.

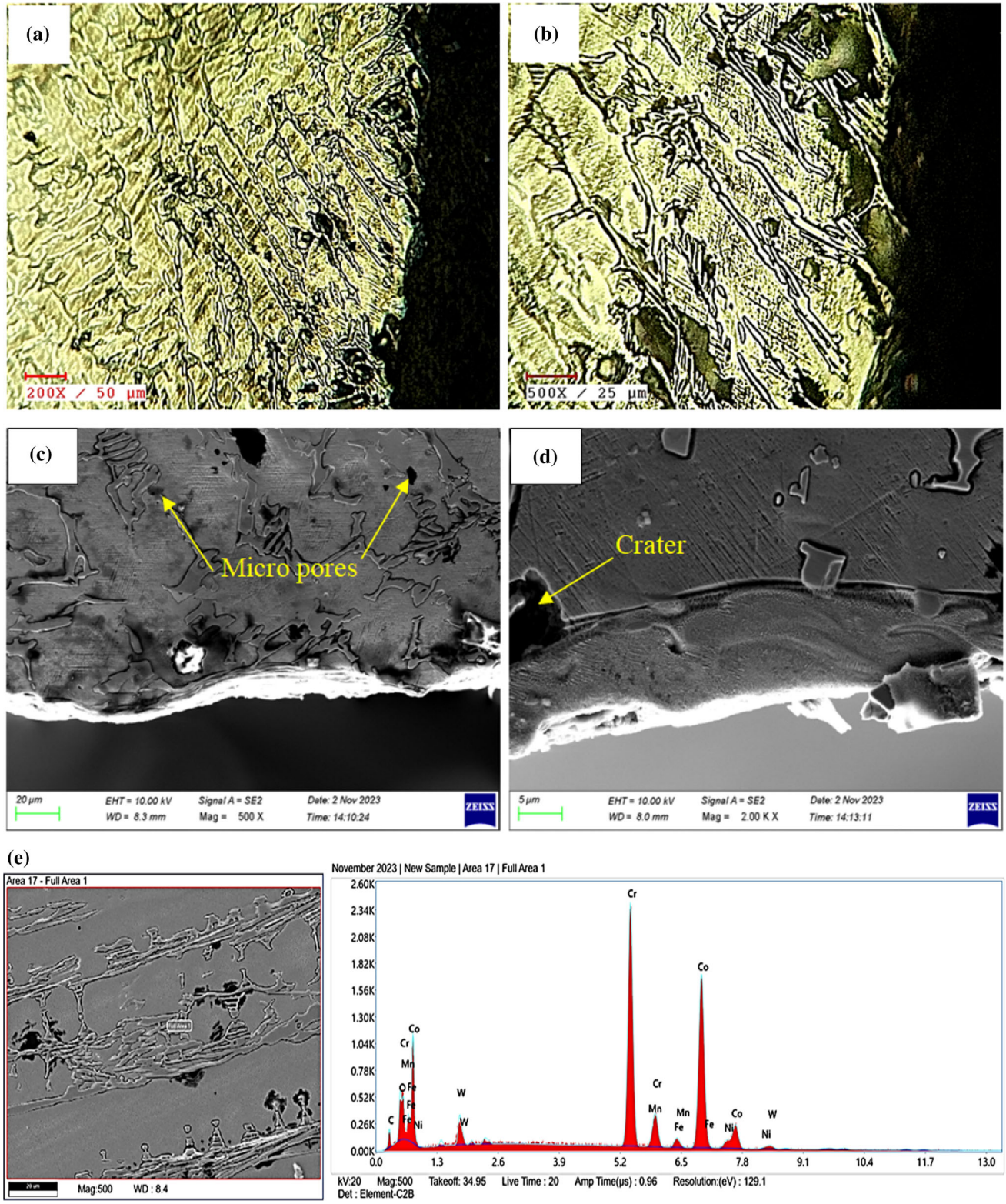

Fig. 13 (a, b) Optical micrographs, (c, d) SEM images, (d) core surface EDS image

During WEDM, heat is generated, and the temperature is approximately 8000-12000 °C, causing local melting and evaporation of the workpiece material. The heat instigates a high-level pressure, but it is insufficient to evacuate all molten materials (Ref 49). The remaining molten material resolidifies on the surface of the machined sample, forming an undulating topography. Upon resolidification of the molten material during the pulse-off time, some gas is entrapped to form microvoids. A high value of applied erosive power caused the formation of a rough surface. These may be the places where individual discharges were able to penetrate far into the workpiece. A

high-energy pulse vaporizes a large amount of metal during the initial discharge.

With increasing pulse-on time, the discharge energy produced will increase; as a result, the brass wire will be accelerated. The residual particles of the brass wire adhere to the cutting surface, resulting in rougher surfaces. Moreover, at higher peak currents, the impact of discharge energy on the surface of the workpiece becomes greater, and thus, the resulting erosion leads to an increase in the deterioration of surface roughness. During machining, a spark erodes a small portion of the workpiece and wire electrode. A portion of this molten material is flushed away by the dielectric medium. The remaining material, which the dielectric is unable to remove, accumulates on the parent material surface, and upon subsequent cooling, the material resolidifies to form a surface layer known as the recast layer (Ref 50). This is the redeposition of the bits of the removed material. Microexplosion also occurs on the machining surface owing to the production of thermal energy in a shorter duration (Ref 51). With increasing pulse-on time, thick debris is formed on the surface. The machined surface quickly reaches the resolidification temperature by the dielectric fluid.

The presence of micropores, craters and melted droplets is attributable to the factuality that the dielectric medium is unable to flush away the melted material due to higher energy discharge, and layer recoil pressure allows the deposition of the debris, furthering the build-up of the recast layer on the workpiece (Ref 52). The formation of craters could be explained by the seizure of discharge, pressure exerted on the molten metal being removed, and expansion of the pressurized gases causing the metal in the molten state to be scattered off the wire surface. With the generation of a greater extent of thermal energy burning, the machined surface and consequently a resolidified lump of mass form on the machined portion (Ref 45, 53).

The microhardness evaluation was carried out using a Vickers hardness tester at a 0.1-kgf load. The hardness profiles of the machined samples exhibiting high MRRs and low Ra values are illustrated in Fig. 14. The microhardness of the recast layers of the samples was measured and found to be in the range of 450-550 Hv (45.3-52.3 HRC), which is considerably greater than the hardness of the base metal 330-430 Hv (33.3-43.6 HRC). The increase in hardness at the recast layer could

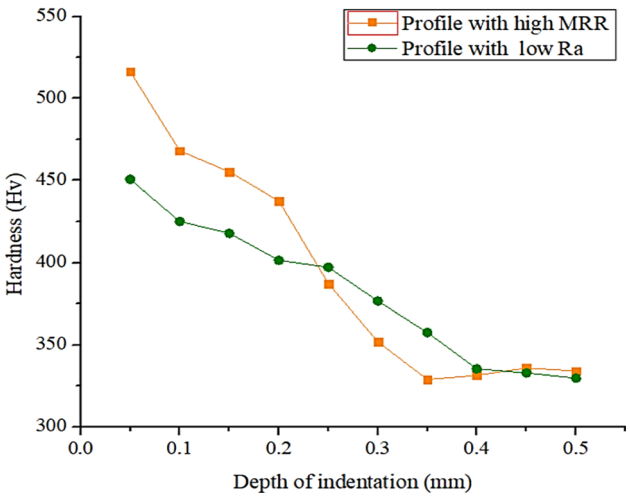

Fig. 14 Hardness profile

be attributed to the primary formation of intermetallic precipitates of chromium carbides ($Cr_{23}C_6$, Cr_7 C_3, $M_{23}C_6$) and tungsten carbide (WC). The presence of carbides contributes significantly to the hardness of the alloy. Additionally, the outermost layer is subjected to cooling via water. Hence, metallurgical transformation occurs due to rapid heating and cooling. This could also be a reason for the higher hardness of the recast layer compared to that of the base alloy (Ref 54).

The decrease in hardness at the recast layer could be ascribed to metallurgical changes. Electrolysis occurs at the dielectric medium, leading to surface oxidation and hence a reduction in surface hardness. The presence of micro-pores and craters constitutes surface irregularities. These surface irregularities result in decreased resistance to plastic deformation, which reduces the hardness (Ref 55). The reduction in hardness indicates that significant thermal degradation occurs on the machined surfaces (Ref 56).

The resolidified layer is relatively non-uniform containing solidified loops. Also, relatively coarser structure below the resolidified material can be seen, accounting for the heat-affected, coarsening of the material. This results in reduction of hardness/strength of the material in the surface region (below the white layer). The surface is spark hardened with the substrate experiencing reduction in hardness possibly due to coarsening of the material and overheating.

4. Conclusion

In this investigation, experimental studies were planned and conducted to observe and predict the effects of cutting parameters on the MRR and Ra during WEDM. It can be confirmed from this work that stellite 6 grade 'B' is fairly machinable using the WEDM process. Optimized process conditions were obtained for two response parameters, MRR and Ra, using multiple objective optimization techniques. The potential implications of the findings are as follows:

- All the factors investigated in this study were found to be significant for their effect on MRR. The contributions of each factor were pulse-on time (27.47%), bed speed (19.47%), peak current (7.59%), pulse-off time (4.57%) and wire feed (1.37%). The optimized input values for the MRR obtained through optimization were 80 μs of pulse-on time, 20 μs of pulse-off time, 2 m/min of wire feed, 5 A of peak current and 20 μm/s of bed speed.
- The optimized input values for Ra obtained through optimization were found to be 60 μs of pulse-on time, 10 μs of pulse-off time, 3 m/min of wire feed, 3 A of peak current and 60 μm/s of bed speed. The contributions of each factor were wire feed (27.78%), bed speed (8.81%), peak current (7.82%), pulse-on time (4.08%) and pulse-off time (1.73%). All of these factors have been found to be significant for their effect on surface roughness, indicating the ability of WEDM to generate highly finished surfaces.
- The MRR, Ra, GRG and fuzzy GRG predictive models are quite precise and may be utilized for predicting the WEDM responses of stellite 6 B alloys. ANOVA revealed that wire feed is the working parameter that has the most influence on the combined responses of GRGs and fuzzy GRGs.
- With regard to the results of multi-objective optimization,

the optimum machining parameters for achieving a higher GRG according to the ANOVA findings are 80 μs of pulse-on time, 10 μs of pulse-off time, 3 m/min of wire feed, 5 A of peak current and 40 μm/s of bed speed.
- The fuzzy approach revealed 60 μs of pulse-on time, 20 μs of pulse-off time, 1 m/min of wire feed, 4 A of peak current and 20 μm/s of bed speed as the optimum conditions for attaining a better grade according to the ANOVA.
- The obtained error percentage among the predicted and experimental GRGs is 17.67%. This observation may be associated with the inherent machining characteristics of the stellite 6 'B' alloy.
- Scanning electron microscopic examination of machined stellite 6 'B' demonstrated the formation of a white recast layer on the order of 10-20 microns with high MRR and low Ra. The microstructure also revealed that the cutting of the samples resulted in the formation of craters and micropores.

References

1. A. Pramanik and G. Littlefair, Machining of Titanium Alloy (Ti-6Al-4V)-Theory to Application, *Mach. Sci. Technol.*, 2015, **19**(1), p 1–49
2. K. Singh, K. Goyal, and D.K. Goyal, Effects of Process Parameters on Material Removal Rate and Surface Roughness in Wedm of H-13 Die Tool Steel, *Adv. Eng. Forum.*, 2018, **28**, p 55–66
3. T. Thankachan, K. Soorya Prakash, and M. Loganathan, WEDM Process Parameter Optimization of FSPed Copper-BN Composites, *Mater. Manuf. Process.*, 2018, **33**(3), p 350–358
4. K.S. Prakash, T. Thankachan, and R. Radhakrishnan, Parametric Optimization of Dry Sliding Wear Loss of Copper–MWCNT Composites, *Trans. Nonferrous Met. Soc. China*, 2017, **27**(3), p 627–637
5. H. Singh, K. Goyal, and P. Kumar, Experimental Investigation of WEDM Variables on Surface Roughness of AISI H13, *Manuf. Sci. Technol.*, 2013, **1**(2), p 23–30
6. K. Mandal, S. Sarkar, S. Mitra, and D. Bose, Parametric Analysis and GRA Approach in WEDM of Al 7075 Alloy, *Mater. Today Proc.*, 2020, **26**, p 660–664
7. A.S. Shivade and V.D. Shinde, Multi-objective Optimization in WEDM of D3 Tool Steel using Integrated Approach of Taguchi Method & Grey Relational Analysis, *J. Ind. Eng. Int.*, 2014, **10**(4), p 149–162
8. R. Chaudhari, J. Vora, D.M. Parikh, V. Wankhede, and S. Khanna, Multi-response Optimization of WEDM Parameters using an Integrated Approach of RSM–GRA Analysis for Pure Titanium, *J. Inst. Eng. India D*, 2020, **101**, p 117–126
9. T. Thankachan, K.S. Prakash, R. Malini, S. Ramu, P. Sundararaj, S. Rajandran, D. Rammasamy, and S. Jothi, Prediction of Surface Roughness and Material Removal Rate in Wire Electrical Discharge Machining on Aluminum Based Alloys/Composites using Taguchi Coupled Grey Relational Analysis and Artificial Neural Networks, *Appl. Surf. Sci.*, 2019, **472**, p 22–35
10. S. Ozturk, Machinability of Stellite-6 Coatings with Ceramic Inserts and Tungsten Carbide Tools, *Arab. J. Sci. Eng.*, 2014, **39**, p 7375–7383
11. Y. Jia, B.S. Kim, D.J. Hu, and J. Ni, Experimental Investigations into Near-Dry Milling EDM of Stellite Alloys, *Int. J. Mach. Mach. Mater.*, 2010, **7**(1–2), p 96–111
12. L. Urtekin, H.B. Ozerkan, C. Cogun, A. Genc, Z. Esen, and F. Bozkurt, Experimental Investigation on Wire Electric Discharge Machining of Biodegradable AZ91 Mg Alloy, *J. Mater. Eng. Perf.*, 2021, **30**(10), p 7752–7761
13. R.S. Gill, K. Kumar, and U. Batra, Surface Characteristics and Corrosion Behaviour of Wire Electrical Discharge Machining Processed Mg-4Zn Alloy, *J. Mater. Eng. Perf.*, 2021, **30**, p 2955–2966
14. N. Kuruvila and H.V. Ravindra, Parametric Influence and Optimization of Wire EDM of Hot Die Steel, *Mach. Sci. Technol.*, 2011, **15**(1), p 47–75
15. N. Tosun, C. Cogun, and A. Inan, The Effect of Cutting Parameters on Workpiece Surface Roughness in Wire EDM, *Mach. Sci. Technol.*, 2003, **7**(2), p 209–219
16. A. Ramamurthy, R. Sivaramakrishnan, T. Muthuramalingam, and S. Venugopal, Performance Analysis of Wire Electrodes on Machining Ti-6Al-4V Alloy using Electrical Discharge Machining Process, *Mach. Sci. Technol.*, 2015, **19**(4), p 577–592
17. S. Tripathy and D.K. Tripathy, Multi-response Optimization of Machining Process Parameters for Powder Mixed Electro-Discharge Machining of H-11 Die Steel using Grey Relational Analysis and Topsis, *Mach. Sci. Technol.*, 2017, **21**(3), p 362–384
18. R. Raju, N. Manikandan, D. Palanisamy, D. Arulkirubakaran, S. Sambathkumar, and P.B. Prakash, Optimization of Process Parameters in Electrical Discharge Machining of Haste Alloy C276 using Taguchi's Method, *Mater. Today Proc.*, 2018, **5**(6), p 14432–14439
19. V. Balaji and S. Narendranath, Influence of Wire-Electric Discharge Machining Process Parameters on Surface Integrity of Ni-rich Ni-Ti-Hf alloys, *Eng. Res. Express*, 2023, **5**, p 025065
20. A. Pramanik, A.K. Basak, M.N. Islam, and G. Littlefair, Electrical Discharge Machining of 6061 Aluminium Alloy, *Trans. Nonferrous Met. Soc. China*, 2015, **25**(9), p 2866–2874
21. S.K. Kar, P.K. Mishra, A.K. Sahu, S.S. Mahapatra, and J. Thomas, Multi-objective Optimization of Wire-EDM of Inconel 625 by using Desirability Function Approach, *Int. J. Interact. Des. Manuf.*, 2023, **17**(2), p 931–938
22. I.V. Manoj, H. Soni, S. Narendranath, P.M. Mashinini, and F. Kara, Examination of Machining Parameters and Prediction of Cutting Velocity and Surface Roughness using RSM and ANN using WEDM of Altemp HX, *Adv. Mater. Sci. Eng.*, 2022, **2022**, p 1–9
23. B.P. Singh, J. Singh, J. Singh, and D. Goyal, Experimental Investigation of Machining Nimonic-80A Alloy on Wire EDM using Response Surface Methodology, *Met. Powder Rep.*, 2021, **76**, p S9–S17
24. R. Bobbili, V. Madhu, and A.K. Gogia, Effect of Wire-EDM Machining Parameters on Surface Roughness and Material Removal Rate of High Strength Armor Steel, *Mater. Manuf. Process.*, 2013, **28**(4), p 364–368
25. M.M. Kane, A.A. Phanse, H.J. Bahirat, and S.V. Kulkarni, Classification and Comparative Study of EDM Pulse Generators, *IET. Power Electron.*, 2020, **13**(14), p 2943–2959
26. A. Goswami and J. Kumar, Trim Cut Machining and Surface Integrity Analysis of Nimonic 80A Alloy using Wire Cut EDM, *Eng. Sci. Tech. Int. J.*, 2017, **20**(1), p 175–186
27. D.A.N. Scott, S. Boyina, and K.P. Rajurkar, Analysis and Optimization of Parameter Combinations in Wire Electrical Discharge Machining, *Int. J. Prod. Res.*, 1991, **29**(11), p 2189–2207
28. C. Balasubramaniyan, K. Rajkumar, and S. Santosh, Wire-EDM Machinability Investigation on Quaternary $Ni44Ti50Cu_4Zr_2$ Shape Memory Alloy, *Mater. Manuf. Process.*, 2021, **36**(10), p 1161–1170
29. D. Deepak, M.C. Gowrishankar, and D.S. Shreyas, Investigation on the Wire Electric Discharge Machining Performance of Artificially Aged Al6061/B_4C Composites by Response Surface Method, *Mater. Res.*, 2022, **25**, p 20220010
30. S. Singh and A. Bhardwaj, Review to EDM by using Water and Powder-Mixed Dielectric Fluid, *J. Miner. Mater. Char. Eng.*, 2011, **10**(02), p 199
31. M. Manjaiah, R.F. Laubscher, A. Kumar, and S. Basavarajappa, Parametric Optimization of MRR and Surface Roughness in Wire Electro Discharge Machining (WEDM) of D2 Steel using Taguchi-Based Utility Approach, *Mech. Mater. Eng. Int. J*, 2016, **11**(1), p 1–9
32. M. Ansari and I.A. Khan, Investigation on the Performance of Wire Electrical Discharge Machining (WEDM) using Aluminium Matrix Composites (AMCs) Micro-Channel, *Eng. Res. Express.*, 2023, **5**(3), p 035065
33. M. Manjaiah, S. Narendranath, and S. Basavarajappa, Wire Electro Discharge Machining Performance of TiNiCu Shape Memory Alloy, *SILICON*, 2016, **8**, p 467–475
34. V.R. Dalve, R. Keshavamurthy, G. Ugrasen, and C.P.S. Prakash, Experimental Investigations on Wire EDM of Al7075-TiB_2 In Situ Metal Matrix Composite, *Appl. Mech. Mater.*, 2014, **592**, p 321–325

35. V. Kavimani, K.S. Prakash, and T. Thankachan, Influence of Machining Parameters on Wire Electrical Discharge Machining Performance of Reduced Graphene Oxide/Magnesium Composite and its Surface Integrity Characteristics, *Compos. B Eng.*, 2019, **167**, p 621–630
36. D. Devarasiddappa and M. Chandrasekaran, Experimental Investigation and Optimization of Sustainable Performance Measures during Wire-Cut EDM of Ti-6Al-4V Alloy Employing Preference-Based TLBO Algorithm, *Mater. Manuf. Process.*, 2020, **35**(11), p 1204–1213
37. A. Mandal, A.R. Dixit, A.K. Das, and N. Mandal, Modeling and Optimization of Machining Nimonic C-263 Superalloy using Multicut Strategy in WEDM, *Mater. Manuf. Process.*, 2016, **31**(7), p 860–868
38. N. Naeim, M.A. AbouEleaz, and A. Elkaseer, Experimental Investigation of Surface Roughness and Material Removal Rate in Wire EDM of Stainless Steel 304, *Materials*, 2023, **16**(3), p 1–16
39. M. Manjaiah, S. Narendranath, S. Basavarajappa, and V.N. Gaitonde, Influence of Process Parameters on Material Removal Rate and Surface Roughness in WED-Machining of Ti50Ni40Cu10 Shape Memory Alloy, *Int. J. Mach. Mach. Mater.*, 2016, **18**(1–2), p 36–53
40. F. Nourbakhsh, K.P. Rajurkar, A.P. Malshe, and J. Cao, Wire Electro-Discharge Machining of Titanium Alloy, *Procedia Cirp.*, 2013, **5**, p 13–18
41. V.K. Pasam, S.B. Battula, P. Madar Valli, and M. Swapna, Optimizing Surface Finish in WEDM using the Taguchi Parameter Design Method, *J. Braz. Soc. Mech. Sci.*, 2010, **32**, p 107–113
42. M.U. Iqbal, J. Santhakumar, and S. Dixit, Multi-objective Optimization of WEDM Process Parameters on Titanium Grade 9 using ANN and Grey Relational Analysis, *AIP Conf. Proc.*, 2022, **2460**(1), p 030008
43. S.A. El-Bahloul, Optimization of Wire Electrical Discharge Machining using Statistical Methods Coupled with Artificial Intelligence Techniques and Soft Computing, *SN Appl. Sci.*, 2020, **2**, p 1–8
44. A. Goyal, H.U. Rahman, and S.A.C. Ghani, Experimental Investigation & Optimisation of Wire Electrical Discharge Machining Process Parameters for Ni49Ti51 Shape Memory Alloy, *J. King Saud Univ. Eng. Sci.*, 2021, **33**(2), p 129–135
45. S.S. Nain, D. Garg, and S. Kumar, Performance Evaluation of the WEDM Process of Aeronautics Super Alloy, *Mater. Manuf. Process.*, 2018, **33**(16), p 1793–1808
46. I.V. Manoj and S. Narendranath, Wire Electric Discharge Machining at Different Slant Angles during Slant Type Taper Profiling of Microfer 4722 Superalloy, *J. Mater. Eng. Perform.*, 2022, **31**(1), p 697–708
47. Y. Wang, D. He, L. Yang, and W. Xiong, Formation Mechanism of Surface Topography in Low-Speed Wire Electrical Discharge Machining Inconel 718 and its On-Line Prediction Based on Acoustic Emission Technology, *Adv. Mech. Eng.*, 2017, **9**(4), p 1–17
48. K. Mouralova, J. Kovar, L. Klakurkova, J. Bednar, L. Benes, and R. Zahradnicek, Analysis of Surface Morphology and Topography of Pure Aluminium Machined using WEDM, *Measurement*, 2018, **114**, p 169–176
49. Y.H. Guu, AFM Surface Imaging of AISI D2 Tool Steel Machined by the EDM Process, *Appl. Surf. Sci.*, 2005, **242**(3–4), p 245–250
50. D. Kumar, K.K.S. Mer, H.S. Payal, and K. Kumar, White-Layer Thickness on Edm-Processed AISI A2 Steel–Mathematical Modeling and Analysis, *Mater. Technol.*, 2022, **56**(2), p 97–106
51. B.E. Kmekci, Residual Stresses and White Layer in Electric Discharge Machining (EDM), *Appl. Surf. Sci.*, 2007, **253**(23), p 9234–9240
52. T.R. Newton, S.N. Melkote, T.R. Watkins, R.M. Trejo, and L. Reister, Investigation of the Effect of Process Parameters on the Formation and Characteristics of Recast Layer in Wire-EDM of Inconel 718, *Mater. Sci. Eng. A*, 2009, **513**, p 208–215
53. G. Ebenezer, M. Adam Khan, D. Chellaganesh, and J. Haider, Assessing Machinability and Surface characteristics of a Shape Memory Alloy (SMA) Processed through Wire Electro Spark Erosion Method, *Arch. Metall. Mater.*, 2022, **67**(3), p 921–930
54. M. Azam, M. Jahanzaib, J.A. Abbasi, M. Abbas, A. Wasim, and S. Hussain, Parametric Analysis of Recast Layer Formation in Wire-Cut EDM of HSLA Steel, *J. Adv. Manuf. Technol.*, 2016, **87**, p 713–722
55. T. Suresh, K. Jayakumar, G. Selvakumar, and S.R. Prakash, Comparative Machining Characteristics Studies on SS 304 using Coated and Uncoated Brass Wire through Wire EDM, *La Metall. Ital.*, p 32-42
56. L. Li, Y.B. Guo, X.T. Wei, and W. Li, Surface Integrity Characteristics in Wire-EDM of Inconel 718 at Different Discharge Energy, *Proc. CIRP*, 2013, **6**, p 220–225